

Chapter 7

Analysis of $B_s^0 \rightarrow \phi\gamma$ and other radiative B decays

S. Barsuk, I. Belyaev, A. Bret, M. Calvo Gomez, O. Deschamps, V. Egorychev, A. Golutvin, R. Graciani Diaz, M. Knecht, A. Kozlinskiy, F. Legger, F. Machefert, I. Machikhiliyan, M-N. Minard, G. Pakhlova, A. Puig Navarro, G. Rospabe, D. Savrina, O. Schneider, K. Senderowska, L. Shchutska, V. Shevchenko, F. Soomro, R. Vazquez Gomez, K. Voronchev, M. Witek, Y. Xie and O. Yushchenko

Abstract

This note presents the roadmap towards the first measurements with radiative modes $B_d^0 \rightarrow K^*\gamma$, $B_s^0 \rightarrow \phi\gamma$ and $B^+ \rightarrow \phi K^+\gamma$ at LHCb. The basic steps toward the first measurements of the radiative decays are presented. We have concentrated on the probing of photon polarization in $B_s^0 \rightarrow \phi\gamma$ decay. Based on our Monte Carlo simulation for 2 fb^{-1} we expect to reach the uncertainty in the measurement of the photon polarization parameter \mathcal{A}^Δ , $\sigma_{\mathcal{A}^\Delta} \approx 0.22$. The capability of the LHCb experiment to measure this and other parameters has been discussed for the different luminosity sets. Several critical aspects and important prerequisites, like calorimeter calibration, implementation of the HLT, determination of proper time acceptance function and γ/π^0 separation at high- E_T have been addressed. The measurements which can be performed already with a data-set of an integrated luminosity of less than 500 pb^{-1} , such as the measurements of the ratio of branching fractions for $B_s^0 \rightarrow \phi\gamma$ and $B^0 \rightarrow K^{*0}\gamma$, and the measurement of the direct \mathcal{CP} -asymmetry for $B^0 \rightarrow K^{*0}\gamma$ decay, are also discussed.

Contents

Introduction	316
1 Radiative penguin decays	318
1.1 Theoretical overview	318
1.2 Experimental Issues	322
2 Current experimental status	325
3 Measurement of the photon polarisation in $B_s^0 \rightarrow \phi\gamma$	327
3.1 Event selection	327
3.2 High Level Trigger	328
3.3 The background	330
3.4 Fit procedure and results	336
3.5 Proper time acceptance function	339
4 The early measurements	350
4.1 The studies with 10 pb^{-1}	350
4.2 The measurements with 100 pb^{-1}	351
4.3 The measurements with 500 pb^{-1} and beyond	354
Summary	355
Appendix A: The observable B_s^0 decay rates	356
Appendix B: The likelihood function for $B_s^0 \rightarrow \phi\gamma$ analysis	357
Appendix C: Calorimeter Calibration	358
Appendix D: Separation of photons and π^0 at high-E_T	367
References	369

Introduction

This note presents the roadmap towards the first measurements of radiative penguin decays of b-hadrons at LHCb using a data-set of an integrated luminosity of up to 2 fb^{-1} . Measurements which require significantly larger integrated luminosities, like, e.g., the measurement of the Cabibbo-suppressed decays $B^0 \rightarrow \rho^0 \gamma$ and $B^0 \rightarrow \omega \gamma$, are not addressed. While the focus of this note is on the measurement of the photon polarisation in $B_s^0 \rightarrow \phi \gamma$ decays, one of the LHCb key measurements which requires the statistics of 2 fb^{-1} , the note also discusses “early” measurements which can be performed already with a data-set of an integrated luminosity of less than 500 pb^{-1} .

A list of interesting measurements with radiative decays of b hadrons includes:

1. the measurement of the photon polarisation and \mathcal{CP} -violation parameters \mathcal{C} and \mathcal{S} in the decay $B_s^0 \rightarrow \phi \gamma$ [1, 2, 3, 4],
2. the measurement of the photon polarisation in the decays of polarised beauty baryons $\Lambda_b \rightarrow \Lambda^0 \gamma$ and $\Lambda_b \rightarrow (\Lambda^* \rightarrow pK^-) \gamma$ [5, 6, 7],
3. the measurement of the photon polarisation in the decay $B^+ \rightarrow \phi K^+ \gamma$,
4. the measurement of direct \mathcal{CP} -violation in the decay $B^0 \rightarrow K^{*0} \gamma$,
5. the precise measurement of the ratio of branching fractions for $B_s^0 \rightarrow \phi \gamma$ and $B^0 \rightarrow K^{*0} \gamma$ decays.

Some of these items have been intensively studied in LHCb [1, 2, 3, 4, 5, 6, 7], while for other topics, e.g. for the decay $B^+ \rightarrow \phi K^+ \gamma$, only the first studies of the event selection have been performed. Table 1 gives the expected nominal event yields for a sample corresponding to 2 fb^{-1} of integrated luminosity and the estimates of the background to signal ratio ($\mathcal{B}_{b\bar{b}}/\mathcal{S}$) for the above mentioned radiative B decays. The measurement of the photon polarisation in the decay $B_s^0 \rightarrow \phi \gamma$ is discussed in Section 3. The measurement of $B^0 \rightarrow K^{*0} \gamma$ and the determination of branching fractions for $B_s^0 \rightarrow \phi \gamma$ and $B^+ \rightarrow \phi K^+ \gamma$ are discussed in Section 4.2.

The most important ingredients and prerequisites which are necessary for the successful measurements of radiative decays and in particular the photon polarisation in $B_s^0 \rightarrow \phi \gamma$ decays include:

- High Level Trigger for events triggered by high energy photons [8];
- the determination of the proper time acceptance function and the resolution function from data;
- the calibration of the LHCb Electromagnetic Calorimeter [9];
- the separation of high energy photons from energetic “merged” π^0 -mesons, misreconstructed as single photons.

Table 1: The expected yields, \mathcal{Y} , per 2 fb^{-1} of integrated luminosity and background to signal ratios, $\mathcal{B}_{b\bar{b}}/\mathcal{S}$, for radiative decays of beauty hadrons. The quoted yields do not include the efficiency of the High Level Trigger, which is expected to be rather high, see Section 3.2. The backgrounds only include backgrounds from $b\bar{b}$ -events. Upper limits are quoted at 90 % CL.

Decay Mode		\mathcal{Y}	$\mathcal{B}_{b\bar{b}}/\mathcal{S}$
$B^0 \rightarrow K^{*0}\gamma$	[2]	7×10^4	$0.6 - 0.7$
$B_s^0 \rightarrow \phi\gamma$	[2]	1.1×10^4	$< 0.6 - 0.9$
$\Lambda_b \rightarrow \Lambda^0\gamma$	[5]	750	< 42
$\Lambda_b \rightarrow \Lambda^0(1670)\gamma$	[5]	2.5×10^3	< 18
$\Lambda_b \rightarrow \Lambda^0(1690)\gamma$	[6]	2.5×10^3	< 18
$\Lambda_b \rightarrow \Lambda^0(1520)\gamma$	[6]	4.3×10^3	< 9
$B^+ \rightarrow \phi K^+\gamma$		$\sim 7 \times 10^3$	$< 2 - 4$

Of course this list is not exhaustive and probably will evolve with time. Only important aspects specific for the radiative decays are listed here. The items of the general interest, like tracking, hadron identification and flavour tagging are discussed elsewhere [10, 11, 12, 13, 14, 15]

This document is organized as follows. In Sections 1 and 2 the current theoretical and experimental status is briefly described. Section 3 describes the measurement of the photon polarisation in $B_s^0 \rightarrow \phi\gamma$ decays. Expected sensitivities are given followed by the discussion of the main systematics. In Section 4 we discuss “early” measurements which on one hand lead already to interesting physics results and on the other hand allow checks of the detector, trigger and reconstruction performance. The important items for successful measurements are described in detail in Sections 3.2 and 3.5, and Appendices C and D.

1 Radiative penguin decays

Radiative decays of b hadrons are an example of flavour changing neutral currents. They are of significant interest due to their sensitivity to new physics and experimental accessibility. The theoretical perspective is given in Section 1.1. The general form of the effective Hamiltonian is used to explain the new physics sensitivity and the dominant source of theoretical uncertainties. The polarisation of emitted photons in radiative decays is found to be particularly worthy of study. The experimental challenges in the study of these processes are described in Section 1.2. This section shows that particular emphasis should be placed on the study of the radiative decays of B_s^0 mesons into a \mathcal{CP} eigenstate.

1.1 Theoretical overview

Radiative decays of b hadrons caused by $b \rightarrow s\gamma$ transition are an interesting example of flavour-changing neutral current processes. From the theoretical point of view the lowest contribution to the amplitude comes from the one-loop process, see Figure 1, and hence, as with any loop process in quantum field theory, the decay pattern may be sensitive to the structure of heavy degrees of freedom of the theory. Another important, while in a sense more technical, reason is that the weak, electromagnetic and perturbative strong parts of the physics behind radiative decays are well under theoretical control. It is also advantageous that one can formulate theoretical predictions for a variety of different observables, such as decay rates, \mathcal{CP} and isospin asymmetries, angular distributions, and cross-check in this way the robustness of the Standard Model (SM) framework. All that places the radiative B decays in the position of “standard candles of flavour physics” [16].

The conventional starting point for the theoretical analysis of B-decays is the effective $\Delta B = 1$ Hamiltonian [17]

$$\mathcal{H}_{\text{eff}} = \frac{G_F}{\sqrt{2}} \sum_{p=u,c} \lambda_p^{(q)} \left(\mathcal{C}_1(\mu) \mathcal{Q}_1^p(\mu) + \mathcal{C}_2(\mu) \mathcal{Q}_2^p(\mu) + \sum_{i=3}^8 \mathcal{C}_i(\mu) \mathcal{Q}_i(\mu) \right), \quad (1.1)$$

where Cabibbo-Kobayashi-Maskawa (CKM) factors are given by $\lambda_p^{(q)} = V_{pq}^\dagger V_{pb}$, and the unitarity relationship has been used. The Wilson coefficients $\mathcal{C}_i(\mu)$ encode physics at mass scales larger than μ (and hence carry information about heavy particles - SM as well as new physics (NP) ones), while matrix elements of hadronic operators $\mathcal{Q}_i(\mu)$ are responsible for long-distance physics dominated by nonperturbative strong interactions. Poor knowledge of these latter factors is the main source of uncertainty of theoretical predictions. At leading order the dominant contribution comes from the electromagnetic penguin operator

$$\mathcal{Q}_7 = -\frac{e}{8\pi^2} \bar{m}_b(\mu) \bar{q} \sigma^{\mu\nu} (1 + \gamma_5) b F_{\mu\nu} \quad (1.2)$$

where $q = d, s$ and $\bar{m}_b(\mu)$ is the $\overline{\text{MS}}$ mass of the b-quark.

The standard theoretical procedure used for evaluation of hadronic matrix elements is based on the QCD factorization idea, augmented by soft-collinear effective theory (for

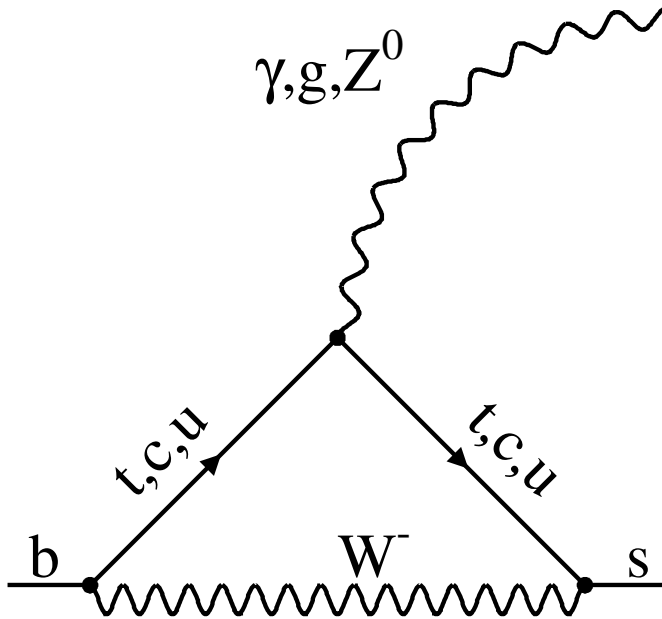


Figure 1: The penguin diagrams for $b \rightarrow s$ transitions.

recent review see [18] and references therein). The latter separates the matrix element of interest into non-perturbative but universal soft functions (form-factors, decay constants, light-cone distribution amplitudes) and hard scattering kernels calculated as perturbative series in α_s . These calculations have been done in next-to-leading and partly in next-to-next-to-leading order [19]. However the whole factorization approach makes sense only in the leading order with respect to the small parameter Λ_{QCD}/m_b and the question of a systematic construction of the $1/m_b$ expansion remains open (see recent discussion in [20]). Needless to say, having reliable SM theoretical predictions is a necessary prerequisite for addressing any NP scenario.

The state-of-the-art theoretical calculation [19] makes predictions for the exclusive branching ratio $B \rightarrow V\gamma$, listed in Table 2. A significant fraction of the uncertainty (about 1/4 of the total) in the branching ratio is due to the poor knowledge of the hadronic form-factor $T_1(B \rightarrow K^*)$ at $q^2 = 0$, but uncertainties from other sources are

Table 2: The theoretical predictions for the branching fractions for exclusive $B \rightarrow V\gamma$ decays [19].

Decay Mode	Branching ratio
$B^+ \rightarrow K^{*+}\gamma$	$(4.6 \pm 1.4) \times 10^{-5}$
$B^0 \rightarrow K^{*0}\gamma$	$(4.3 \pm 1.4) \times 10^{-5}$
$B_s^0 \rightarrow \phi\gamma$	$(4.3 \pm 1.4) \times 10^{-5}$

also important.

When discussing possible NP scenarios in the low energy effective Hamiltonian language, it is useful to distinguish those where only short-distance functions $\mathcal{C}_i(\mu)$ get modified with respect to the SM predictions and those where the structure of terms in the right hand side of Eq. (1.1) changes, for example, because new operators $\mathcal{Q}_i^{\text{NP}}$ (absent in the SM) appear. The models of the first sort are of “minimal flavour violating” type [21] since the only source of quark flavour mixing in this case is the CKM matrix of the SM. In a sense they are the most difficult to discover. The reason is clear: our ability to disentangle these scenarios crucially depends on the uncertainties in hadronic matrix elements, since the latter limits the accuracy of $\mathcal{C}_i^{\text{exp}}$ extracted from experimental data which we are interested in comparing with theoretical SM predictions of $\mathcal{C}_i^{\text{th}}$. The most prominent way of reducing this uncertainty seems to be further development of sophisticated numerical computations on the lattice, which is now the main tool of getting nonperturbative QCD results with the error budget under control. We refer interested readers to recent talks at the Lattice 2008 conference [22] where the current status of computations of hadronic matrix elements relevant for B decays is thoroughly reviewed. In short, we find ourselves in a peculiar situation: to discover minimal flavour violating NP in B decays of the discussed type we need to make progress in hardware and algorithms to get better knowledge of nonperturbative hadronic quantities (notably the form-factor $T_1(B \rightarrow K^*)$) rather than to obtain more precise experimental results for exclusive branching ratios, since the error is already dominated by theory. But even with the lattice accuracy reached so far, experimental data on $B \rightarrow K^*\gamma$ and other radiative penguin decays already put strong constraints on many models available on the theoretical market. The main qualitative message can be stated as follows: all observed branching ratios are generally consistent with each other and with the SM predictions and there is no doubt that the SM loop process depicted in Figure 1 is responsible for the main contribution to the radiative b decay.

It would however be wrong to conclude from the arguments presented above that rare radiative decays are not sensitive probes of NP and deserve no attention in this respect. The crucial point is that besides such a crude tool as branching ratios more complex information can be extracted from various \mathcal{CP} asymmetries, time-dependent rates, angular distributions, isospin asymmetries and other quantities of analogous character. It is clear that if one considers non-minimally flavour violation scenarios with new operators and new complex phases, the choice of NP-sensitive observables becomes wider and typically for each particular beyond SM scenario one can distinguish observables most fit to search for it. For example, the theory prediction for the isospin asymmetry

$$\mathcal{A}_{B \rightarrow K^*\gamma}^I = \frac{\Gamma(\bar{B}^0 \rightarrow \bar{K}^{*0}\gamma) - \Gamma(B^- \rightarrow K^{*-}\gamma)}{\Gamma(\bar{B}^0 \rightarrow \bar{K}^{*0}\gamma) + \Gamma(B^- \rightarrow K^{*-}\gamma)}$$

is sensitive to the operator \mathcal{Q}_6 and hence provides constraints on corresponding NP [23]. In what follows we concentrate on another important class of observables related to the photon polarization, where a crucial contribution is expected from LHCb.

We can express the Hamiltonian for $b \rightarrow s\gamma$ in the following form:

$$\Delta\mathcal{H} = -\sqrt{8}G_F \frac{e\bar{m}_b}{16\pi^2} \mathcal{F}_{\mu\nu} \left[\mathcal{A}_L \bar{s}\sigma^{\mu\nu} \frac{1+\gamma_5}{2} b + \mathcal{A}_R \bar{s}\sigma^{\mu\nu} \frac{1-\gamma_5}{2} b \right] + \text{h.c.} \quad (1.3)$$

Here $\mathcal{A}_L(\mathcal{A}_R)$ corresponds to the amplitude for the emission of left (right) handed photons in the $b \rightarrow s_L\gamma_L(b \rightarrow s_R\gamma_R)$ decays. This can be easily seen by writing the electromagnetic field tensor for left (right) polarized photons as: $\mathcal{F}_{\mu\nu}^{L,R} = \frac{1}{2}(\mathcal{F}_{\mu\nu} \pm i\tilde{\mathcal{F}}_{\mu\nu})$, where $\tilde{\mathcal{F}}_{\mu\nu} = \frac{1}{2}\varepsilon_{\mu\nu\sigma\rho}\mathcal{F}^{\sigma\rho}$. Using the identity $\sigma_{\mu\nu}\gamma_5 = \frac{i}{2}\varepsilon_{\mu\nu\alpha\beta}\sigma^{\alpha\beta}$, one can see that only the $\mathcal{F}_{\mu\nu}^L$ part survives in the first term of the right-hand side of Eq. (1.3) and only $\mathcal{F}_{\mu\nu}^R$ in the second one. In the SM the amplitude ratio, representing the fraction of “wrong” helicity photons $\mathcal{A}_R/\mathcal{A}_L$ is proportional to the mass ratio m_s/m_b , since in the SM only the left-handed components of the external fermions couple to the W boson. Thus the leading contribution is given by the operator of Eq. (1.2). This naive m_s/m_b scaling can however be destroyed by corrections, which take into account gluon emission. This effect may affect significantly the purity of the photon polarization. In papers [24] and [25] these contributions were estimated to be sufficiently large, about 10 %, however these results were based mainly on dimensional estimations. More precise calculations in perturbative QCD, taking into account the effects from hard gluon emission in the main part, give a contribution on the level of 3-4 % [26]. The nonperturbative corrections from the soft gluon emission via the c-quark loop, induced by the \mathcal{O}_2 -operator, turn out to be about 1 %, nonperturbative contributions from the annihilation diagrams and other operators are of the same order or smaller as can be seen from the light cone sum rule method calculations [27]. Thus we conclude, following original arguments from [28], that the polarization of emitted photons in radiative decays is a good example of a nontrivial experimental observable sensitive to the Lorentz structure of effective Hamiltonian operator containing the photon emission vertex.

The admixture of photons with the “wrong” polarization may be rather large in some SM extensions like e.g. the Left Right Symmetric Model (LRSM). Here the enhancement of the right-handed photon fraction is due to $W_L - W_R$ mixing, and chirality flip along the internal t-quark line in the loop leads to a large factor m_t/m_b in the amplitude for producing right-handed photons. It was shown that within the unconstrained minimal supersymmetric model (uMSSM) a strong enhancement of order $m_{\tilde{g}}/m_b$ is possible due to chirality flip along the gluino line and left-right squark mixing. In this case the degree of photon polarization, λ_γ , defined as

$$\lambda_\gamma = \frac{|\mathcal{A}_R|^2 - |\mathcal{A}_L|^2}{|\mathcal{A}_R|^2 + |\mathcal{A}_L|^2} \quad (1.4)$$

can take any value between -1 and 1 [29]. The model with anomalous right-handed top couplings [30] also allows sizeable contributions in \mathcal{A}_R , $-1 \leq \lambda_\gamma \leq -0.12$.

In models with non-supersymmetric extra dimensions there are also no reasons for the right-handed photon to be suppressed with respect to the left-handed one, so that in the general case left-handed and right-handed amplitudes are comparable and mixing-induced

\mathcal{CP} asymmetries are of the order of one [31]. Thus the information one can get in this way is extremely interesting providing a typical example of a “null test” [32], since the photons are almost 100 % polarized in the SM.

1.2 Experimental Issues

The experimental challenge therefore is to measure the amplitude ratio $\left| \frac{\mathcal{A}(\text{B} \rightarrow \Phi \gamma_{\text{R}})}{\mathcal{A}(\text{B} \rightarrow \Phi \gamma_{\text{L}})} \right|$ where Φ represents some final hadronic state. There is no experimental possibility to measure photon polarization directly, but there are several indirect strategies. The first one is the study of angular distributions of the Φ decay products [33, 34]. In this way one is able to measure only the square of the amplitude ratio. Indeed, using the definition of the photon polarization parameter λ_γ from Eq. (1.4) one has

$$\frac{d\Gamma(\text{B} \rightarrow \Phi \gamma)}{d\Omega} \propto (|\mathcal{A}_{\text{R}}|^2 + |\mathcal{A}_{\text{L}}|^2) + \lambda_\gamma (|\mathcal{A}_{\text{R}}|^2 - |\mathcal{A}_{\text{L}}|^2). \quad (1.5)$$

It is worth noticing that the amplitudes $\mathcal{A}_{\text{R,L}}$ corresponding to left-handed and right-handed photons do not interfere in this case since the polarization of the photon in the final state can (at least in principle) be measured independently. By studying the angular distribution one can extract λ_γ from Eq. (1.5), in other words the method makes use of angular correlations among the decay products¹ in $\text{B} \rightarrow [\Phi \rightarrow \text{P}_1 \text{P}_2 \text{P}_3] \gamma$, where P_i is either a pion or a kaon. This technique was originally suggested in [33, 34] and used for the decay $\text{B} \rightarrow \text{K} \pi \pi \gamma$ with the sum over intermediate hadronic resonances. The radiative decay mode $\text{B} \rightarrow [\varphi \rightarrow \text{K}^+ \text{K}^-] \text{K} \gamma$ is considered in [35]. This mode is rather distinctive with many desirable features from the experimental point of view: the final state is a photon plus only charged mesons (for charged B mesons), the fact that φ is narrow reduces the effects of intermediate resonances interference, etc. However the actual situation is rather involved. The possibility of measuring λ_γ in this way depends on a delicate partial-wave interference pattern. The latter may be unfavourable and the asymmetry may escape detection [35].

Alternatively, one can study baryon decays $\Lambda_{\text{b}} \rightarrow \Lambda^0 \gamma \rightarrow \text{p} \pi \gamma$ (or $\Lambda_{\text{b}} \rightarrow \Lambda^* \gamma \rightarrow \text{p} \text{K} \gamma$) and measure the photon polarization via the forward-backward asymmetry of the proton with respect to the Λ_{b} in the Λ^0 rest frame for polarized Λ_{b} , (see [36, 37, 38] for details and references therein).

Aside from the experimental difficulties, the main problem of these two methods is the absence of interference between the amplitudes, corresponding to left- and right-handed photon emission, since they correspond to different and distinguishable (at least in principle) final states. Correspondingly they are sensitive only to the square of the amplitude ratio in the form of λ_γ , see Eq. (1.4). It would be advantageous to measure (the absolute value of) the amplitude ratio as it is. There are two possible ways to do that. The first one makes use of the fact that some photons convert in the detector material into electron-positron pairs. Thus it is possible to have the desired interference.

¹Notice that there must be at least three particles in the final state.

It can be shown that for these processes the distribution in the angle ϕ between the e^+e^- plane and the plane defined by the final state hadrons (e.g. $K\pi$ resulting from K^* decay) should be isotropic for purely circular polarization, while the deviations from this isotropy includes the same parameter $\mathcal{A}_R/\mathcal{A}_L$, indicating the presence of right-handed photons [39, 40, 41, 42]. However multiple scattering does not allow to identify the decay plane for the low invariant mass e^+e^- -pair. This is not the case for pair creation from virtual photons where one can select pair masses above 30 MeV/ c^2 without losing too much rate. However in this case other diagrams contribute with longitudinal virtual photons. The LHCb prospects for this measurement are discussed elsewhere [43].

Another way is to study the time evolution of $B_{(s)}^0 \rightarrow \Phi^{CP}\gamma$ decays, where Φ^{CP} is some CP -eigenstate. In this case the time-dependent decay rate can be conventionally parameterized as follows:

$$\Gamma_{B_{(s)}^0 \rightarrow \Phi^{CP}\gamma}(t) = |A|^2 e^{-\Gamma_{(s)}t} \left(\cosh \frac{\Delta\Gamma_{(s)}t}{2} - \mathcal{A}^\Delta \sinh \frac{\Delta\Gamma_{(s)}t}{2} + \mathcal{C} \cos \Delta m_{(s)}t - \mathcal{S} \sin \Delta m_{(s)}t \right) \quad (1.6a)$$

$$\Gamma_{\bar{B}_{(s)}^0 \rightarrow \Phi^{CP}\gamma}(t) = |A|^2 e^{-\Gamma_{(s)}t} \left(\cosh \frac{\Delta\Gamma_{(s)}t}{2} - \mathcal{A}^\Delta \sinh \frac{\Delta\Gamma_{(s)}t}{2} - \mathcal{C} \cos \Delta m_{(s)}t + \mathcal{S} \sin \Delta m_{(s)}t \right) \quad (1.6b)$$

Within the SM one has [44]:

$$\begin{aligned} \mathcal{C} &\approx 0 \\ \mathcal{S} &\approx \sin 2\psi \sin \varphi_{(s)} \\ \mathcal{A}^\Delta &\approx \sin 2\psi \cos \varphi_{(s)}, \end{aligned} \quad (1.7)$$

where ψ is defined as

$$\tan \psi \equiv \left| \frac{\mathcal{A}(\bar{B}_{(s)} \rightarrow \Phi^{CP}\gamma_R)}{\mathcal{A}(\bar{B}_{(s)} \rightarrow \Phi^{CP}\gamma_L)} \right| \quad (1.8)$$

and related to the fraction of “wrongly”-polarized photons²; and $\varphi_{(s)}$ is the sum of $B_{(s)}^0$ mixing phase and CP -odd weak phases for right \mathcal{A}_R and left \mathcal{A}_L amplitudes. From Eqs. (1.7) and (1.8) one can see that the measurement of \mathcal{A}^Δ and \mathcal{S} directly determines the “wrongly”-polarized photon fraction [44].

For the B^0 system the parameter $\Delta\Gamma$ is negligible, and as a result the terms proportional to \mathcal{A}^Δ vanish:

$$\Gamma_{B^0 \rightarrow \Phi^{CP}\gamma}(t) \approx |A|^2 e^{-\Gamma t} (1 - \mathcal{S} \sin \Delta m t) \quad (1.9a)$$

$$\Gamma_{\bar{B}^0 \rightarrow \Phi^{CP}\gamma}(t) \approx |A|^2 e^{-\Gamma t} (1 + \mathcal{S} \sin \Delta m t) \quad (1.9b)$$

²Note that the parameter λ_γ , defined by Eq. (1.4) could be expressed as $\lambda_\gamma = \cos 2\psi$.

Also in the SM one expects $\sin \varphi = \sin(2\beta - \phi_p) \approx \sin 2\beta$, where ϕ_p is \mathcal{CP} -odd weak penguin phase. Therefore one gets:

$$\mathcal{S}_{B^0} = \sin 2\psi \sin 2\beta. \quad (1.10)$$

On the contrary for the B_s^0 system the parameter $\Delta\Gamma_s$ is not negligible, providing a non-zero sensitivity to \mathcal{A}^Δ . In the SM φ_s is expected to be small, $\sin \varphi_s = \sin(2\beta_s - \phi_p) \approx 0$, thus the term with \mathcal{S} vanishes:

$$\Gamma_{B_s^0 \rightarrow \Phi \mathcal{CP} \gamma}(t) \approx |A|^2 e^{-\Gamma_s t} \left(\cosh \frac{\Delta\Gamma_s t}{2} - \mathcal{A}^\Delta \sinh \frac{\Delta\Gamma_s t}{2} \right) \quad (1.11a)$$

$$\Gamma_{\bar{B}_s^0 \rightarrow \Phi \mathcal{CP} \gamma}(t) \approx \Gamma_{B_s^0 \rightarrow \Phi \mathcal{CP} \gamma}(t) \quad , \quad (1.11b)$$

and finally one gets:

$$\mathcal{A}_{B_s^0}^\Delta \approx \sin 2\psi, \quad (1.12)$$

thus opening the possibility for the direct measurement of the photon polarization parameter $\sin 2\psi$ [45]. It is worth to stress here that for vanishing \mathcal{S} and \mathcal{C} , both B_s^0 and \bar{B}_s^0 exhibit the same decay-time evolution and therefore no flavour tagging is required for extraction of $\sin 2\psi$.

2 Current experimental status

Exclusive radiative B decays have been measured by the CLEO, BABAR, and Belle experiments. The first measurement of a radiative B decay was the measurement of the branching ratio of $B \rightarrow K^* \gamma$ by the CLEO collaboration [46]. Today the $B^0 \rightarrow K^{*0} \gamma$ signal can serve as a reference point for the measurement of other radiative decays and as a calibration signal. Its branching fraction is well measured by all three collaborations. The current measurements are summarized in Table 3. Within the SM the direct \mathcal{CP} -asymmetry for this decay is predicted to be less than 1 % [47]. No evidence of a deviation from this prediction has been seen in the measured charge asymmetry for the exclusive B^\pm and B^0 decays to $K^* \gamma$, see Table 3.

Table 3: The branching fraction for the decay $B^0 \rightarrow K^{*0} \gamma$ and the direct \mathcal{CP} -violation asymmetry for the decay $B^0 \rightarrow K^{*0} \gamma$ measured at the B factories.

Experiment		$\mathcal{B}(B^0 \rightarrow K^{*0} \gamma)$ [10^{-6}]	$\mathcal{A}_{\mathcal{CP}}(B \rightarrow K^* \gamma)$
BABAR	[48]	$39.2 \pm 2.0 \pm 2.4$	$-0.013 \pm 0.036 \pm 0.010$
Belle	[49]	$40.1 \pm 2.1 \pm 1.7$	$-0.015 \pm 0.044 \pm 0.012$
CLEO	[50]	$45.5^{+7.2}_{-6.8} \pm 3.4$	$+0.08 \pm 0.13 \pm 0.03$
PDG'08 & HFAG	[51, 52]	40.1 ± 2.0	-0.010 ± 0.028

The $B^+ \rightarrow \phi K^+ \gamma$ decay mode was observed first by the Belle collaboration [53] and the branching fraction has been measured both by the Belle and BABAR collaborations, see Table 4.

Table 4: Branching fractions for $B^+ \rightarrow \phi K^+ \gamma$ and $B_s^0 \rightarrow \phi \gamma$ decays.

Experiment		$\mathcal{B}(B^+ \rightarrow \phi K^+ \gamma)$ [10^{-6}]	$\mathcal{B}(B_s^0 \rightarrow \phi \gamma)$ [10^{-6}]
Belle		$3.4 \pm 0.9 \pm 0.4$	$57^{+18}_{-15}(\text{stat})^{+12}_{-11}(\text{syst})$ [54]
BABAR		$3.5 \pm 0.6 \pm 0.4$	—
PDG'08	[51]	3.5 ± 0.6	$< 120@90 \text{ \%CL}$
HFAG	[52]	3.5 ± 0.6	57^{+21}_{-18}

The direct asymmetry for this decay is reported by BABAR collaboration to be $\mathcal{A}_{\mathcal{CP}} = -0.26 \pm 0.14 \pm 0.05$ [55]. Recently the Belle collaboration also observed for the first time a radiative penguin decay of the B_s meson: $B_s^0 \rightarrow \phi \gamma$. The measured branching fraction was found to be in agreement with the SM expectations and the branching fraction for the $B^0 \rightarrow K^{*0} \gamma$ decay.

The measurement of the photon polarization in $b \rightarrow s \gamma$ transitions allows to search for right-handed FCNC and provides a powerful probe to test SM. The effects of photon polarization have been studied by BABAR and Belle through the measurement of time-dependent \mathcal{CP} -asymmetries for $B^0 \rightarrow (K^{*0} \rightarrow K_S^0 \pi^0) \gamma$, $B^0 \rightarrow K_S^0 \pi^0 \gamma$, $B^0 \rightarrow \eta K^0 \gamma$, $B^0 \rightarrow$

$K_S^0 \rho^0 \gamma$ and $B^0 \rightarrow \rho^0 \gamma$ decays. The results for the parameters \mathcal{C} and \mathcal{S} defined in (1.9) for these decays are summarized in Table 5.

Table 5: The \mathcal{CP} -violation parameters \mathcal{C} and \mathcal{S} measured for various exclusive radiative decays.

Experiment		$\mathcal{C}(B^0 \rightarrow K^{*0} \gamma)$	$\mathcal{S}(B^0 \rightarrow K^{*0} \gamma)$
BABAR	[56]	$-0.14 \pm 0.16 \pm 0.03$	$-0.03 \pm 0.29 \pm 0.03$
Belle	[57]	$0.20 \pm 0.24 \pm 0.05$	$-0.32_{-0.33}^{+0.36} \pm 0.05$
		$\mathcal{C}(B^0 \rightarrow K_S^0 \pi^0 \gamma)$	$\mathcal{S}(B^0 \rightarrow K_S^0 \pi^0 \gamma)$
BABAR	[56]	$0.36 \pm 0.33 \pm 0.04$	$-0.78 \pm 0.59 \pm 0.09$
Belle	[57]	$0.20 \pm 0.20 \pm 0.06$	$-0.10 \pm 0.31 \pm 0.07$
		$\mathcal{C}(B^0 \rightarrow \eta K^0 \gamma)$	$\mathcal{S}(B^0 \rightarrow \eta K^0 \gamma)$
BABAR	[58]	$-0.32_{-0.39}^{+0.40} \pm 0.07$	$-0.18_{-0.46}^{+0.49} \pm 0.12$
		$\mathcal{C}(B^0 \rightarrow K_S^0 \rho^0 \gamma)$	$\mathcal{S}(B^0 \rightarrow K_S^0 \rho^0 \gamma)$
Belle	[59]	$-0.05 \pm 0.18 \pm 0.06$	$-0.11 \pm 0.33_{-0.09}^{+0.05}$
		$\mathcal{C}(B^0 \rightarrow \rho^0 \gamma)$	$\mathcal{S}(B^0 \rightarrow \rho^0 \gamma)$
Belle	[60]	$0.44 \pm 0.49 \pm 0.14$	$-0.83 \pm 0.65 \pm 0.18$

Using Eq. (1.10) and taking $\sin 2\beta = 0.678 \pm 0.025$ [51], one finds for the current precision of the single most precise measurement of $\sin 2\psi$ in $B^0 \rightarrow K^{*0} \gamma$ decay:

$$\sigma_{\sin 2\psi}^{B^0 \rightarrow K^{*0} \gamma} = 0.43, \quad (2.1)$$

where ψ is defined through the ratio of amplitudes by Eq. (1.8).

3 Measurement of the photon polarisation in $B_s^0 \rightarrow \phi\gamma$

The measurement of the photon polarisation in $B_s^0 \rightarrow \phi\gamma$ events can be done either through the measurement of the $\mathcal{A}^\Delta \sinh \frac{\Delta\Gamma_s t}{2}$ or the $\mathcal{S} \sin \Delta m_s t$ -terms, of Eq. (1.6) (see also Appendix A). The measurement of the amplitude of $\sinh \frac{\Delta\Gamma_s t}{2}$ -terms can be done with untagged events. It is practically insensitive to the proper time resolution [3], but requires the knowledge of the proper time acceptance function, see Section 3.5. In contrast, the measurement of the amplitude of the fast oscillating $\sin \Delta m_s t$ -term requires flavour tagging and is limited mainly by the proper time resolution [3] and has only a modest dependency on the uncertainty of the proper time acceptance function.

The relative amplitude of the oscillating term with respect to the term proportional to $\sinh \frac{\Delta\Gamma_s t}{2}$ is about $1.5(1 - 2\omega) \varepsilon^{\text{tag}} \tan \varphi_s$ at $\tau = \tau_{B_s^0}^0$ and drops quickly to about $0.1(1 - 2\omega) \varepsilon^{\text{tag}} \tan \varphi_s$ at $\tau = 3\tau_{B_s^0}^0$, where $\tau_{B_s^0}^0$ is the nominal lifetime of B_s^0 meson [51], ε^{tag} is the flavour tagging efficiency, ω is mistag rate, and φ_s is the difference between the B_s^0 mixing phase and the weak phase of penguin amplitude, see Eqs. (1.6) and (A.1).

Taking this into account we concentrate on the measurement of photon polarisation through the measurement of \mathcal{A}^Δ .

3.1 Event selection

The event selection criteria described in detail elsewhere [2], have been chosen to maximize the ratio $\frac{\mathcal{S}}{\sqrt{\mathcal{S} + \mathcal{B}}}$. The reconstruction efficiency ε_{rec} , selection efficiency for reconstructed events $\varepsilon_{\text{sel/rec}}$, the L0-trigger efficiency for selected events $\varepsilon_{\text{L0/sel}}$ and the total efficiency ε_{tot} are summarized in Table 6.

Assuming the nominal detector performance we expect to observe $B_s^0 \rightarrow \phi\gamma$ signal mass peak with effective resolution of 98 MeV/ c^2 , see Figure 2 [2,3]. The width is dominated by the resolution of the Electromagnetic calorimeter [1, 2, 9], see Appendix C. The expected statistics for $B^0 \rightarrow K^{*0}\gamma$ and $B_s^0 \rightarrow \phi\gamma$ decays for the accumulated luminosity of 2 fb⁻¹ (see Table 1) will allow us to perform the precise measurement of the actual signal shape from data.

Table 6: The reconstruction efficiency ε_{rec} , selection efficiency for reconstructed events $\varepsilon_{\text{sel/rec}}$ and the L0-trigger efficiency for selected $B_s^0 \rightarrow \phi\gamma$ events $\varepsilon_{\text{L0/sel}}$ [2].

Efficiency	$B_s^0 \rightarrow \phi\gamma$
ε_{rec}	1.9%
$\varepsilon_{\text{sel/rec}}$	11.7%
$\varepsilon_{\text{L0/sel}}$	44.1%
ε_{tot}	0.10%

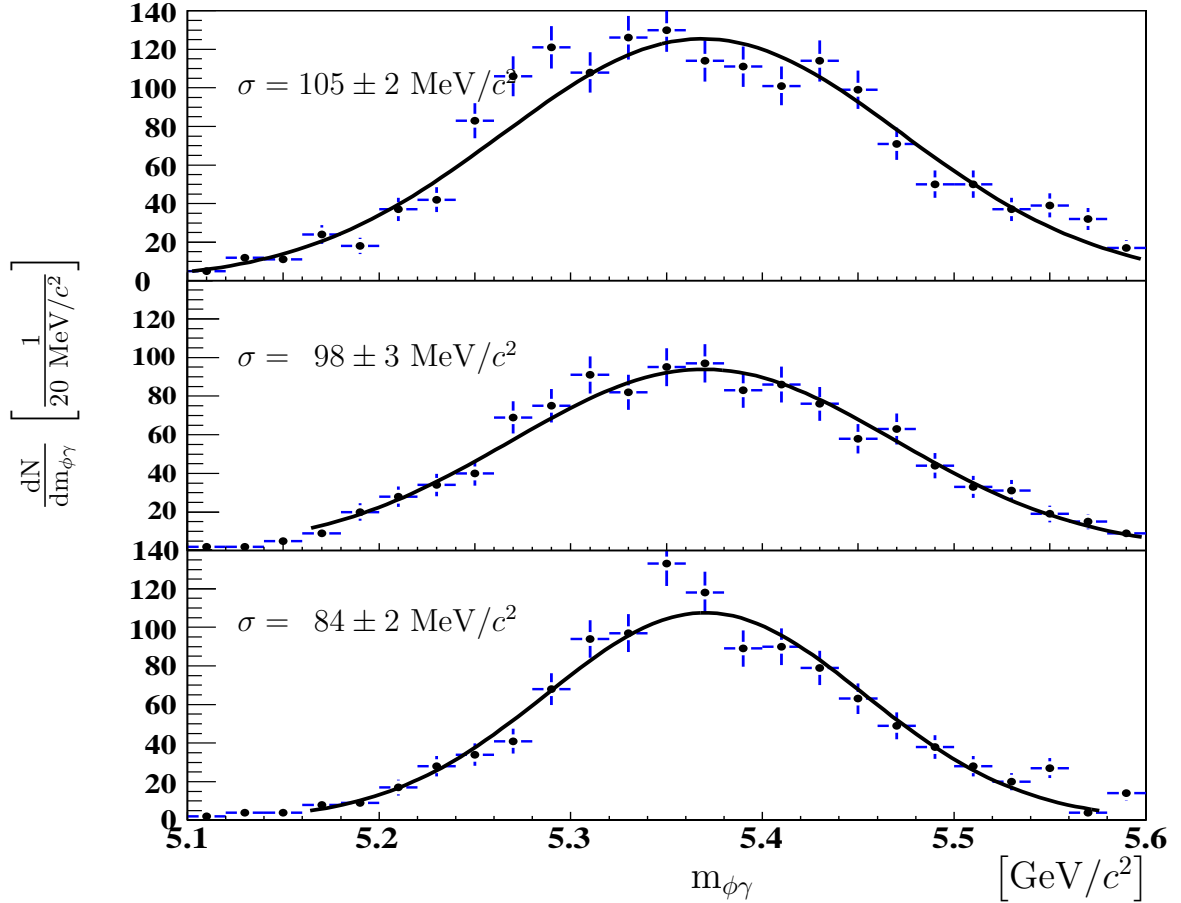


Figure 2: Signal invariant mass distribution after selection cuts for photons, detected in inner, middle and outer (from top to bottom) zones of the Electromagnetic Calorimeter. The curves represent the fit with a Gaussian signal function. The effective resolution for all three zones together is $98 \pm 2 \text{ MeV}/c^2$.

The proper time resolution for the signal events can be described by a sum of two Gaussian functions³ with the resolutions of 52 ± 5 and 114 ± 7 fs, and the fraction of narrow component of 51 ± 9 %, see Figure 3.

3.2 High Level Trigger

The structure of the High Level Trigger line for events triggered by high transverse energy photons is described in detail elsewhere [8]. In brief, the algorithm can be sketched as follows. The sequence of the photon HLT line begins with the confirmation of the L0

³ The B_s^0 proper time resolution is dominated by the ϕ -vertex resolution. The vertex is reconstructed with two kaon tracks and the error on its position depends strongly on the opening angle between two kaons. In particular it increases with the decreasing of the angle between the ϕ and the B_s^0 flight direction in the B_s^0 rest frame [1, 3].

$$\frac{dN}{d(\tau^{\text{REC}} - \tau^{\text{MC}})} \left[\frac{1}{33 \text{ fs}} \right]$$

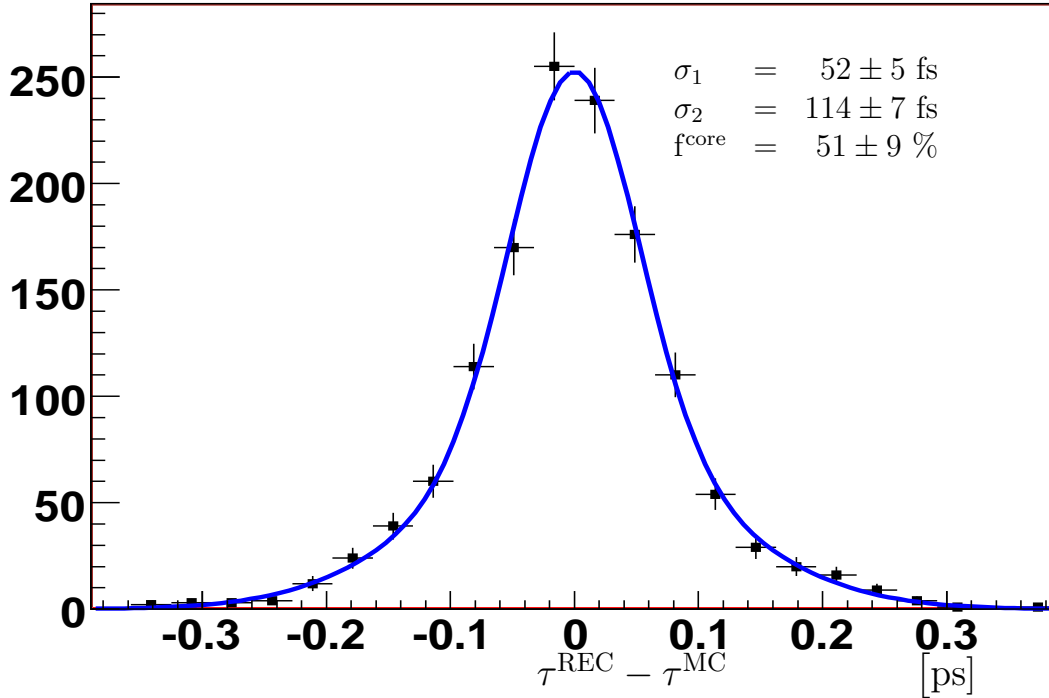


Figure 3: The proper time resolution for the $B_s^0 \rightarrow \phi\gamma$ events passing all selection criteria [3]. The curve represents the fit with a double Gaussian function. The effective resolutions are 52 ± 5 and 114 ± 7 fs and the fraction of the narrow component is 51 ± 9 %.

photon candidate. A fast clusterization is performed in the Ecal region close to the L0 photon candidate. The closest Ecal cluster with compatible energy is selected for subsequent analysis. A set of cluster shape variables is calculated to remove clusters which come from merged π^0 . This reduces the minimum bias rate by a factor of 2 while preserving 90 % of the signal events. Then the 2D-Velo reconstruction is launched and 2D-Velo tracks with 2D-impact parameters in excess of $100 \mu\text{m}$ are selected for 3D-Velo reconstruction. The 3D-tracks with impact parameter in excess of $150 \mu\text{m}$ are reconstructed in the tracker stations behind the magnet and at least one track is required to have large transverse momentum $p_T > 700 \text{ MeV}/c$. The reduced bandwidth after this step allows a full 3D-Velo reconstruction. The companion track is searched among all 3D-Velo tracks. The ones with distance of closest approach less than $200 \mu\text{m}$ are reconstructed in the tracker stations and kept if their transverse momentum is larger than $700 \text{ MeV}/c$. Then the two track vertex is formed, and a requirement on vertex quality is imposed. In the last step the photon is added to the vertex without additional cuts. Figure 4 illustrates the performance of the HLT1 line for $B_s^0 \rightarrow \phi\gamma$ events.

The efficiency of the first step of the High Level Trigger $\varepsilon_{\text{HLT1}}$ has been estimated to be around 70 % at 10 kHz minimum bias rate. It is worth to note here that for the HLT1 the option “*photon + single track*” instead of (or, in addition to) the option “*photon +*

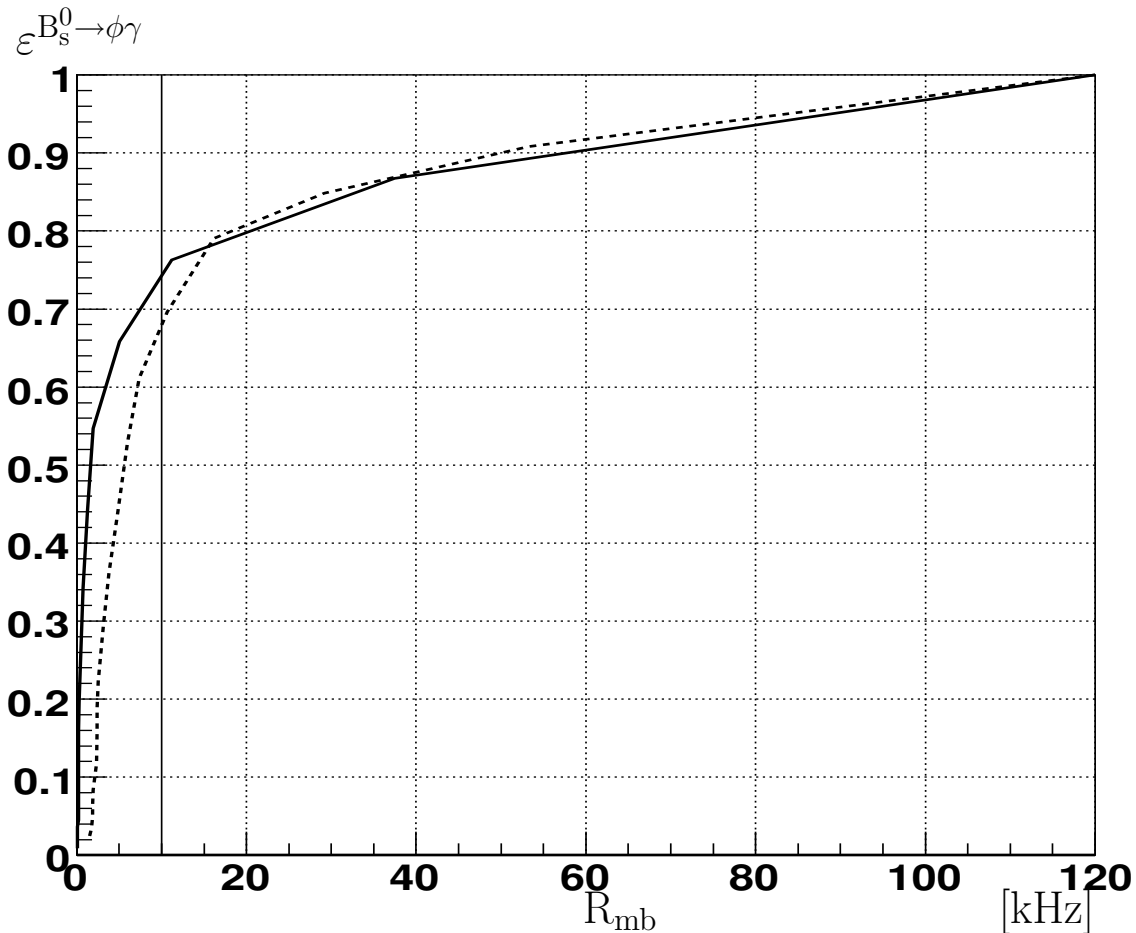


Figure 4: HLT1 efficiency $\varepsilon^{B_s^0 \rightarrow \phi\gamma}$ for selected events versus minimum bias rate R_{mb} for two HLT1 strategies: “*photon + two tracks*” (solid line) and “*photon + single track*” (dotted line).

two tracks” is still open.

For the next trigger step (HLT2) the full reconstruction of the $B_s^0 \rightarrow \phi\gamma$ candidate is performed with relaxed cuts, compared to those used in the final selection. An efficiency of 90% has been found for a minimum bias background rate of 16 Hz. Also, the “inclusive ϕ ” trigger line, which selects the detached $\phi \rightarrow K^+K^-$ vertices, has an efficiency of 77% for $B_s^0 \rightarrow \phi\gamma$ events.

3.3 The background

Possible backgrounds have been studied in detail both for $B_s^0 \rightarrow \phi\gamma$ and $B^0 \rightarrow K^{*0}\gamma$ modes using slightly relaxed selection criteria to increase the event statistics [2]. The major part of the background consists of the random combination of two tracks from the same secondary vertex together with a merged π^0 -meson, misidentified as a single high energy photon. Using a dedicated π^0/γ -separation algorithm, see Appendix D, this major

fraction of background can be significantly reduced.

Peaking background from badly reconstructed decays $B_s^0 \rightarrow \phi\pi^0$ where the energetic “merged” π^0 is misreconstructed as a photon, is expected to be small, since this decay is highly suppressed⁴. Even without γ/π^0 -separation the cut on the polarisation of the vector meson drastically reduces this potential feed-down [1]. Assuming $\mathcal{B}(B_s^0 \rightarrow \phi\pi^0) = \mathcal{B}(B^0 \rightarrow K^{*0}\pi^0)$, and using the recent upper limit $\mathcal{B}(B^0 \rightarrow K^{*0}\pi^0) < 3.5 \times 10^{-6}$ [51] the final contribution from this source is expected to be less than 0.4% at 90% confidence level⁵.

Another background which potentially leads to a contribution in the signal mass region is misreconstructed events $B^0 \rightarrow K^{*0}\gamma$ where the pion from the $K^{*0} \rightarrow K^+\pi^-$ decay is misidentified as a kaon. For a small fraction of such events the invariant mass of the true and fake kaon falls into the narrow mass window around the nominal ϕ meson mass. A Monte Carlo study shows that for this background the central value of the reconstructed mass is shifted by $\sim 100 \text{ MeV}/c^2$ upwards with respect to the nominal mass of B_s^0 meson and its width is about 2-3 times wider. However, the absolute contribution is negligible and amounts to 0.3 % even in case of a 100 % misidentification of pions as kaons, see Figure 5.

Parameterization of the background as function of reconstructed proper time and reconstructed mass

The shape of the background mass distribution obtained with the limited Monte Carlo statistics is consistent with an exponential behaviour $\propto e^{-\mu m_{\phi\gamma}}$ with the parameter $\mu = 0.8 (\text{GeV}/c^2)^{-1}$, see Figure 6 [3].

More generally the background as a function of the reconstructed invariant mass can be described as:

$$f_b(m_{\phi\gamma}) \propto e^{-\mu m_{\phi\gamma}} \times P(m_{\phi\gamma}), \quad (3.1)$$

where $P(m_{\phi\gamma})$ is a smooth function (e.g. low-order polynomial) of the reconstructed invariant mass.

A crucial point of the analysis is the ability to extract the shape of the background under the signal using the sidebands. It has been demonstrated that the simultaneous fit of left and right sidebands, defined as 4.4–5.1 GeV/c^2 and 5.7–6.4 GeV/c^2 correspondingly, allows the precise determination of the background parameters [3].

Important for the analysis is the parameterization of the background distribution as a function of the reconstructed proper time. This parameterization can be extracted from the invariant mass sidebands. The nature of the background events in the low and high mass sidebands is different and one therefore expects different reconstructed proper time distributions for events of the left and right sidebands. Using a very general ansatz the

⁴This isospin-violating decay proceeds through a gluonic penguin graph, which in turn preserves isospin.

⁵This contribution has been estimated to be less than 4 % in reference [1] using $\mathcal{B}(B^0 \rightarrow K^{*0}\pi^0) < 3.6 \times 10^{-5}$.

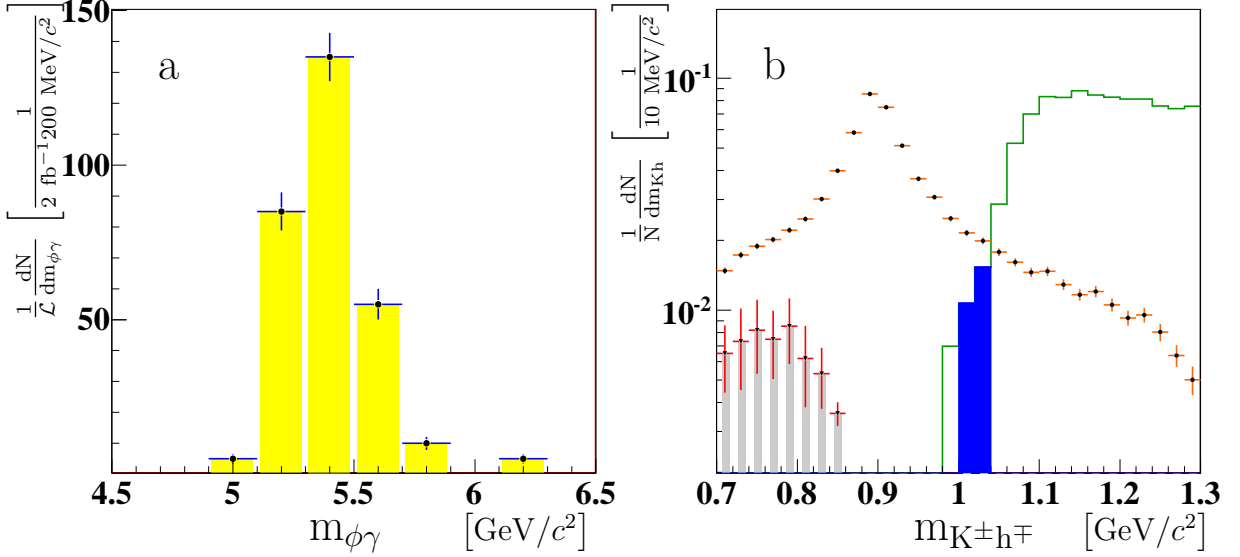


Figure 5: a) The absolute contribution of the feed-down from $B^0 \rightarrow K^{*0}\gamma$ decays misreconstructed as $B_s^0 \rightarrow \phi\gamma$ signal events for 2 fb^{-1} . b) The distribution of the $K\pi$ invariant mass from $B^0 \rightarrow K^{*0}\gamma$ decays (points with errors) and the corresponding mass distribution in case the pion is identified as second kaon (open histogram). The solid blue histogram shows the fraction of these misidentified K^+K^- combinations, consistent with the mass window used for selecting ϕ candidates. The light grey histogram with error bars shows the original $K\pi$ invariant mass of the wrongly identified ϕ events. A 100 % misidentification of pions as kaons has been assumed for these plots.

background proper time distribution can be expressed as:

$$f_b(t) \propto \epsilon_{B_s^0 \rightarrow \phi\gamma}(t) \sum_i f_i e^{-t/\tau_i}, \quad (3.2)$$

where the common factor $\epsilon_{B_s^0 \rightarrow \phi\gamma}(t)$ is the proper time acceptance function for the signal decay $B_s^0 \rightarrow \phi\gamma$, which is assumed to be known in this section and is discussed in Section 3.5. A Monte Carlo study shows that the proper time acceptance can be parameterized as:

$$\epsilon_{B_s^0 \rightarrow \phi\gamma}(t) \propto \frac{(at)^c}{1 + (at)^c}. \quad (3.3)$$

The parameters have been found⁶ to be [3]:

$$\begin{aligned} a &= 0.74 \pm 0.09 \text{ ps}^{-1} \\ c &= 1.86 \pm 0.15, \end{aligned}$$

see Figures 7 and 8.

⁶With a larger Monte Carlo sample more precise estimates for these parameters have been obtained, see (3.7).

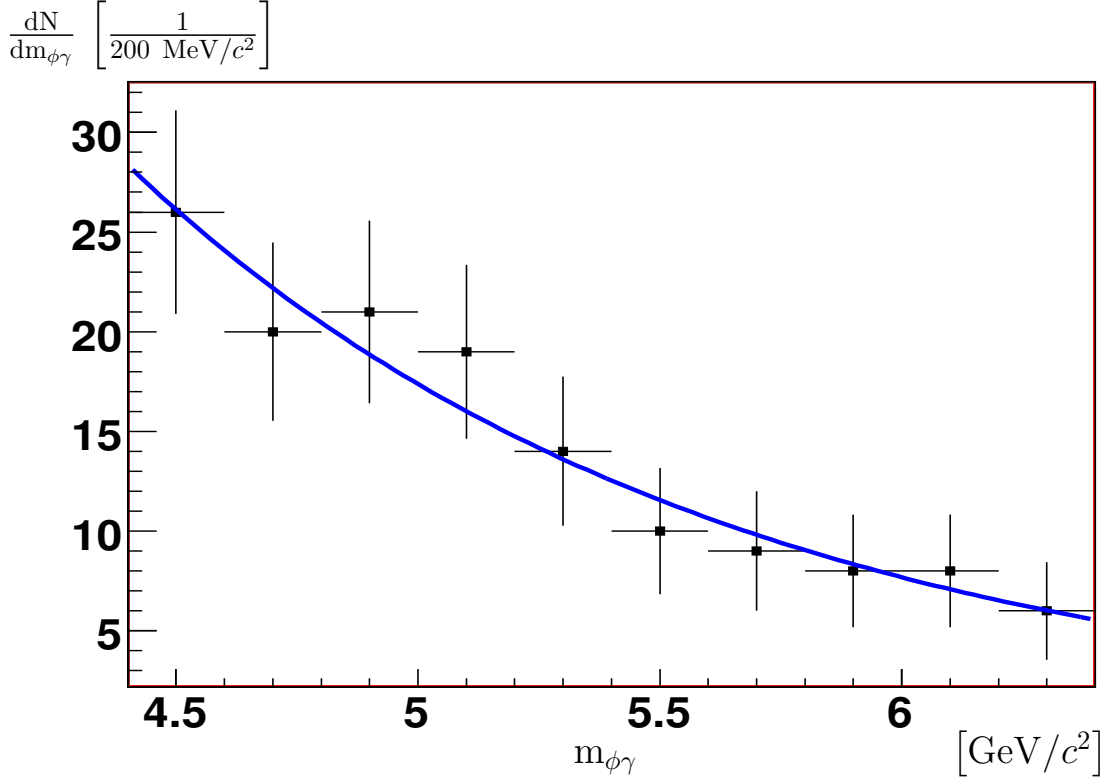


Figure 6: $b\bar{b}$ -inclusive background mass distribution after relaxed selection for limited Monte Carlo statistics [3]. The curve represents the fit with an exponential function.

One can perform the fits of the left and right sidebands separately with the function (3.2) to determine the parameters f_i and τ_i of the different background components. In practice it is more convenient to perform the fit of the sum of the left and right sidebands to determine the leading exponential factors τ_i and only then perform the separate fits of the left and right sidebands using the common set of τ_i to determine the relative composition f_i for two sidebands separately (f_i^L for the left sideband and f_i^R for the right sideband respectively). For the limited Monte Carlo data samples it has been shown [3] that two exponential functions are enough to describe both left and right sidebands, see Figures 9 and 10.

The time parameters τ_i were determined from a fit to simulated background distributions (see Figures 9 and 10) and were found to be 0.45 ps and 8.7 ps. The decay time of short and long lived background component are significantly smaller and significantly larger than the nominal lifetime of B_s meson [51] correspondingly⁷.

The coherent description of the background events as a function of two variables, the reconstructed mass of the B_s candidate and its proper time, is achieved by combining the separate parameterizations (3.1) and (3.2) assuming a smooth dependence of coefficients f_i from (3.2) on the reconstructed mass $m_{\phi\gamma}$: $f_i \longrightarrow f_i(m_{\phi\gamma})$. With such a substitution

⁷Probably due to these large differences the resulting uncertainties on the physics parameters \mathcal{A}^Δ , \mathcal{C} and \mathcal{S} were found to be almost insensitive with respect to the actual composition of the background [3].

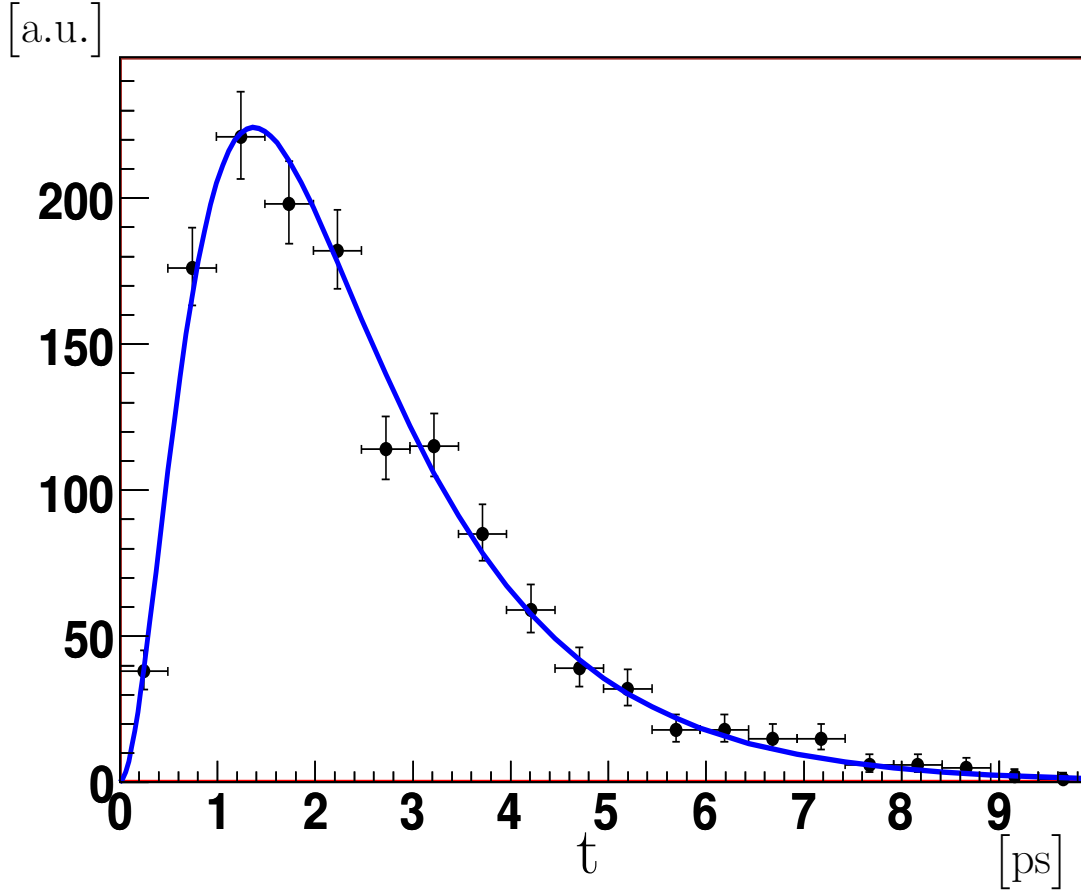


Figure 7: The proper time distribution for $B_s^0 \rightarrow \phi\gamma$ events [3] fitted with the function $f(t) = e^{-t/\tau} \epsilon_{B_s^0 \rightarrow \phi\gamma}(t)$, where $\epsilon_{B_s^0 \rightarrow \phi\gamma}(t)$ is defined by Eq. (3.3).

the distribution of the background as a function of two variables can be written as

$$f_b(m_{\phi\gamma}, t) \propto [e^{-\mu m_{\phi\gamma}} P(m_{\phi\gamma})] \times [\epsilon_{B_s^0 \rightarrow \phi\gamma}(t) \sum_i f_i(m_{\phi\gamma}) e^{-t/\tau_i}], \quad (3.4)$$

where the first part is a function of reconstructed mass only, and describes the leading dependence of $f_b(m_{\phi\gamma}, t)$ on the reconstructed mass $m_{\phi\gamma}$, and the second part has a rather modest dependence on the reconstructed mass but is responsible to describe the dependency on the reconstructed proper time. A linear parameterization of $f_i(m_{\phi\gamma})$ has been used:

$$f_i(m_{\phi\gamma}) = f_i^0 + \delta f_i(m_{\phi\gamma} - m_{B_s}) \quad (3.5)$$

The parameters f_i^0 and δf_i could be calculated from the values f_i^L and f_i^R determined from the two sidebands separately. Instead of using the functions (3.4) and (3.5) a simultaneous fit to the low-mass and high-mass sideband regions in the $(m_{\phi\gamma}, t)$ -plane has been performed. It turned out that choosing the simplest expression for $P(m_{\phi\gamma}) = 1$ and the linear parameterization of f_i a sufficiently good description of the time behaviour

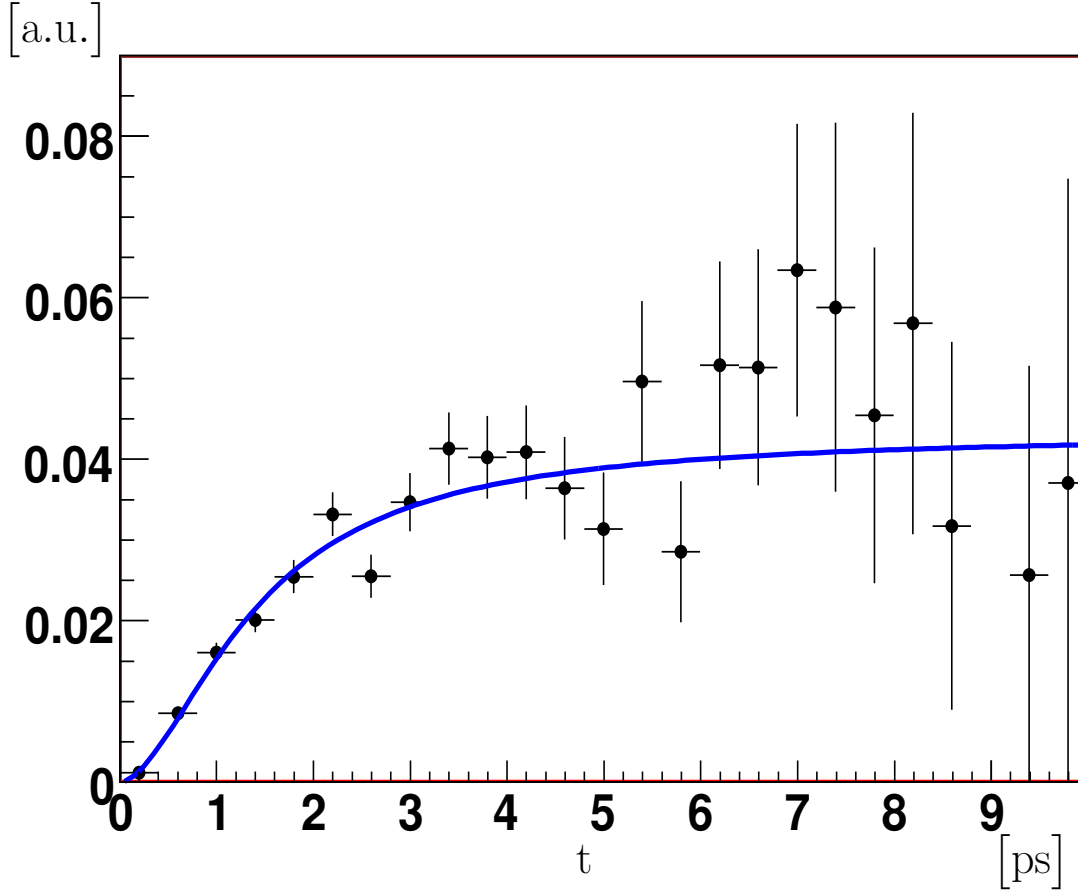


Figure 8: The proper time acceptance $\epsilon_{B_s^0 \rightarrow \phi\gamma}(t)$ for $B_s^0 \rightarrow \phi\gamma$ events fitted with the function (3.3) [3].

is achieved. As shown in Table 7 all necessary background parameters are well determined [3].

The convergence of the fit can be improved using proper initial values, determined from the previous one-dimensional fits. However if some parameter from the fit where all parameters are left free tends to differ from the initial (and expected) value, this case requires a separate detailed investigation, as well as the case of a bad fit quality when all parameters fixed at their expected values. This could be a signature of some of the basic assumptions not being valid. For example it could indicate that the simple linear model (3.5) is not valid and one needs to use more complicated dependencies, e.g. a second order polynomial:

$$f_i(m_{\phi\gamma}) = f_i^0 + \delta f_i(m_{\phi\gamma} - m_{B_s}) + f_i''(m_{\phi\gamma} - m_{B_s})^2.$$

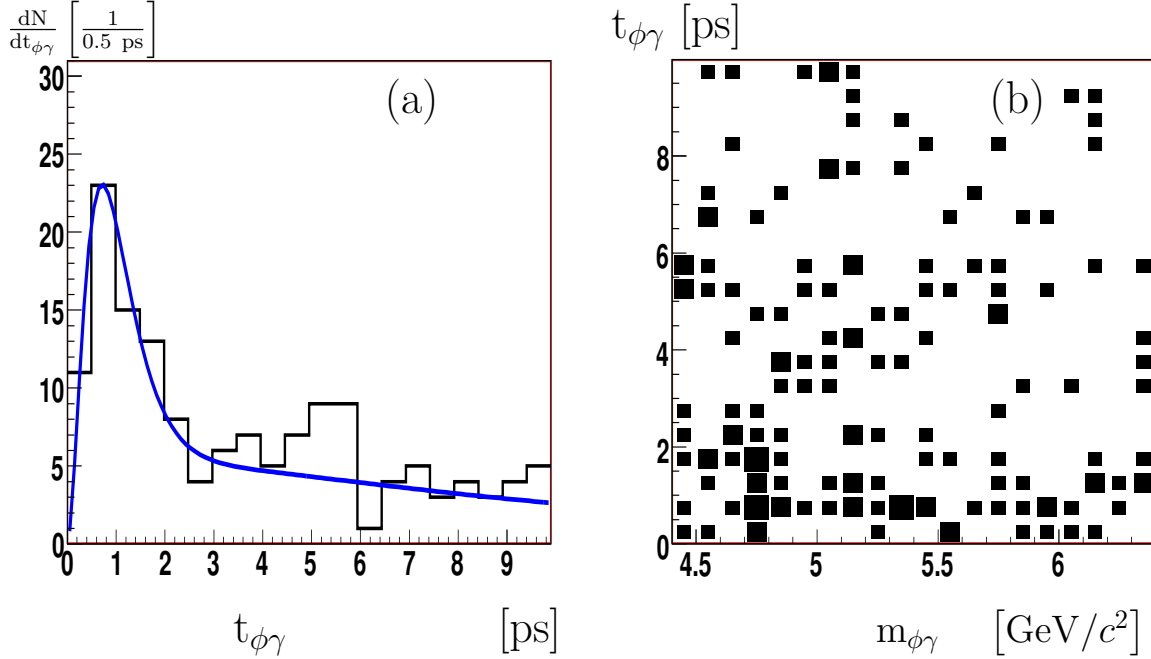


Figure 9: a) Proper time distribution of background events; b) proper time vs. invariant mass distribution for $b\bar{b}$ -inclusive events after the relaxed selection cuts.

3.4 Fit procedure and results

After a detailed study and verification of the background parameterization models (3.4), using the low-mass and high-mass sideband regions in the $(m_{\phi\gamma}, t)$ -plane, one can start the usual procedure of the unbinned maximum likelihood fit. The construction of the simplest likelihood function is described in Appendix B. We are planning to use the technique of blind analysis and instead of the physical parameter \mathcal{A}^Δ use some linear function $\mathcal{A}_{\text{blind}}^\Delta = \alpha\mathcal{A}^\Delta + \beta$, with “unknown” parameters α and β .

We are going to start with the fit ignoring the tagging information. All parameters, including the normalization of signal and background, except $\mathcal{A}_{\text{blind}}^\Delta$ could be fixed at their expected values. The result of this fit needs to be compared with the result of the fit where the background parameters are kept free⁸.

Also, we are planning to perform series of fits where the generic signal parameters,

⁸Probably here one can also use free parameters for the signal normalization.

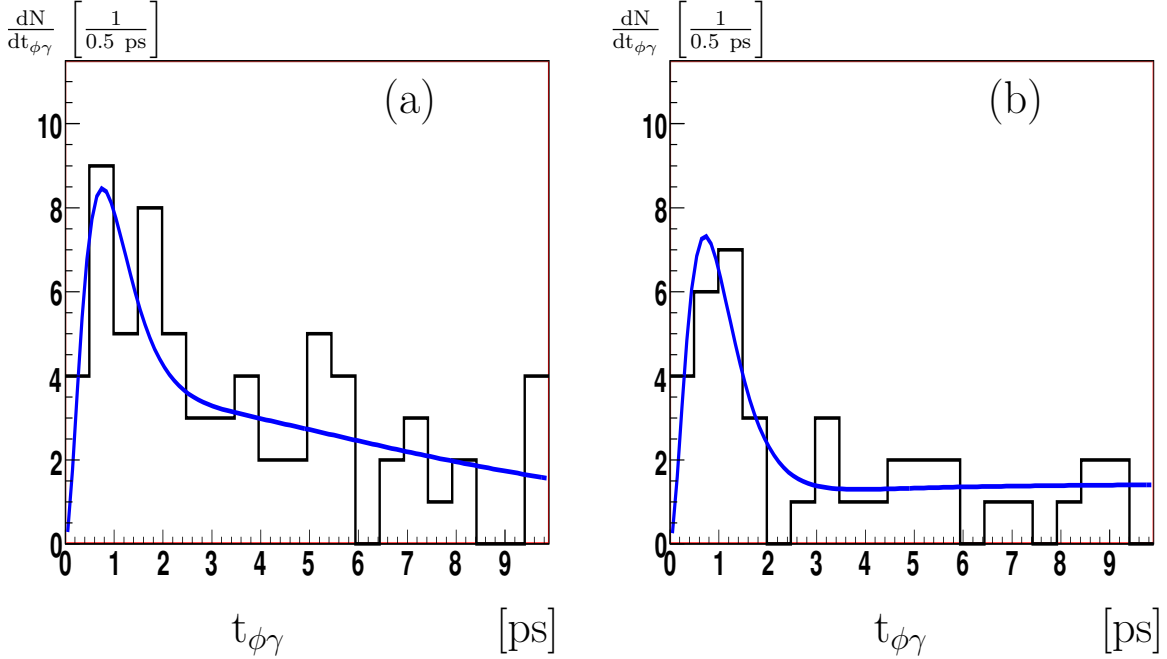


Figure 10: Proper time distribution of background events [3]: a) for left-sideband region with invariant mass 4.4–5.1 GeV/ c^2 ; b) for right-sideband region with invariant mass 5.7–6.4 GeV/ c^2 .

like the nominal lifetime of the B_s meson, and the value of $\Delta\Gamma_s$ are allowed to vary ⁹.

It is worth to note here that $\Delta\Gamma_s$ must be fixed or constrained in the fit using external measurements, e.g., the precise measurements from $B_s^0 \rightarrow \phi J/\psi$ channel, where $\Delta\Gamma_s$ is expected to be measured with 6-8 % precision [10].

For fits of the considered proper lifetime range and the loose constraint on $\Delta\Gamma_s$ possible variations in the nominal lifetime of the B_s meson are absorbed in $\Delta\Gamma_s$ and $\mathcal{A}_{\text{blind}}^\Delta$, without affecting the background parameterizations. In a similar way variations of $\Delta\Gamma_s$, either as a fixed or constraint parameter, are absorbed by the released lifetime of B_s meson and $\mathcal{A}_{\text{blind}}^\Delta$, without affecting the shape of the background.

Toy Monte Carlo studies [3,4] show that the uncertainty on parameter \mathcal{A}^Δ for the fit procedure that we are planning to use in the first measurement (not using the tagging information) is the same as in case of the combined analysis exploiting the flavour tagging

⁹Since for small $\Delta\Gamma_s$ the expression (1.11) looks as:

$$\Gamma_{B_s^0 \rightarrow \phi c \bar{c} \gamma}(t) \approx |A|^2 e^{-\Gamma_s t} \left[1 - \frac{\mathcal{A}^\Delta \Delta\Gamma_s t}{2} + \frac{1}{2} \left(\frac{\Delta\Gamma_s t}{2} \right)^2 + \dots \right] \quad (3.6)$$

we are sensitive mainly to the product $(\mathcal{A}^\Delta \Delta\Gamma_s)$, and the obtained value of $\mathcal{A}_{\text{blind}}^\Delta$ should have a very strong dependence on the value of $\Delta\Gamma_s$ used. However, for these series of fits we do not care about the value of $\mathcal{A}_{\text{blind}}^\Delta$.

Table 7: The errors on the background shape parameters obtained from 2D simultaneous fit of the low-mass and high-mass sideband regions on the on the $(m_{\phi\gamma}, t)$ -plane for statistics equivalent to 2 fb^{-1} of integrated luminosity. The values of input parameters are specified in the column “Input value”. The parameter $c_1^0 = 1$ is fixed.

Parameter	Input/Expected Value	Error
c_1^0	1	—
δc_1	0.041	0.20
$1/\tau_1$	2.23	0.04
c_2^0	0.025	0.0014
δc_2	-0.007	0.004
$1/\tau_2$	0.118	0.005

information¹⁰. The distribution of the fitted values of \mathcal{A}^Δ for $\mathcal{O}(10^4)$ toy experiments, each of them equivalent to 2 fb^{-1} of accumulated data is shown in Figure 11. The expected uncertainty has been estimated to be ~ 0.22 for a $\frac{\Delta\Gamma_s}{\Gamma_s}$ value of 0.12 [3].

The fitted values of \mathcal{A}^Δ are practically unbiased and the errors returned by the fit are reliable. Figure 12 shows the corresponding pull distribution.

The expected statistical uncertainty for \mathcal{A}^Δ is independent of the value of \mathcal{A}^Δ and scales with square root of the luminosity: $\sigma_{\mathcal{A}^\Delta} \propto \mathcal{L}^{-\frac{1}{2}}$ [4]. In case of a combined fit of tagged and untagged events the parameter \mathcal{A}^Δ is found to be independent of the parameters \mathcal{S} and \mathcal{C} : the correlation coefficients do not exceed 2 % [3,4]. The uncertainties and corresponding pulls are summarized in Table 8.

The result of a toy experiment with $\mathcal{A}^\Delta = 0.4$ for a data set equivalent to 2 fb^{-1} of accumulated data is shown in Figure 13.

¹⁰ For flavour tagging the following parameters have been used: the tagging efficiency $\epsilon^{\text{tag}} = 0.610 \pm 0.002$ and the mistag rate $\omega = 0.30$ [3,4,15]. A single tagging category has been assumed here. Considering multiple tagging categories has the potential to improve the results on \mathcal{S} and \mathcal{C} parameters which depend on the tagging [15].

Table 8: The uncertainties for parameters \mathcal{A}^Δ , \mathcal{C} , and \mathcal{S} from the combined fit of tagged and untagged samples and the corresponding pull parameters, obtained for $\mathcal{O}(10^4)$ toy experiments, each of them equivalent to 2 fb^{-1} of accumulated data.

Parameter	Uncertainty	Pull mean	Pull sigma
\mathcal{A}^Δ	0.217 ± 0.002	0.03 ± 0.01	1.03 ± 0.01
\mathcal{C}	0.115 ± 0.001	0.01 ± 0.01	1.08 ± 0.01
\mathcal{S}	0.114 ± 0.001	0.02 ± 0.01	1.00 ± 0.01

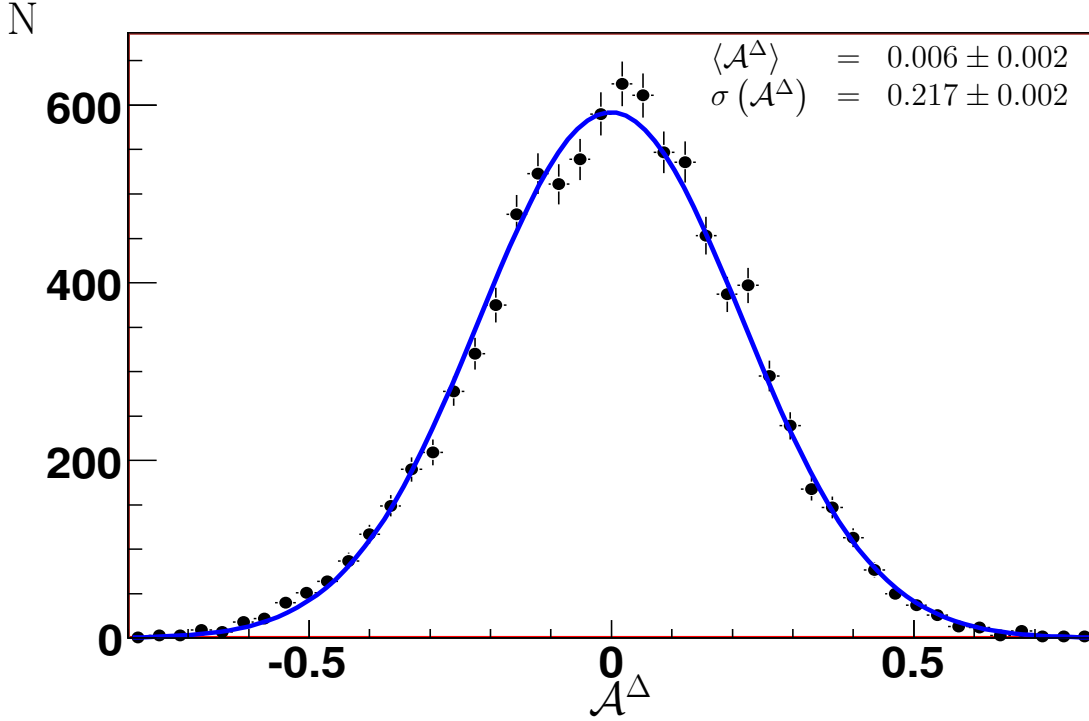


Figure 11: The distributions of fit results for \mathcal{A}^Δ for $\mathcal{O}(10^4)$ toy experiments, where $\mathcal{A}^\Delta = 0$ has been used as input value. The curve shows a Gaussian fit, with mean value 0.006 ± 0.002 and width 0.217 ± 0.002 .

3.5 Proper time acceptance function

The determination of the proper time acceptance function is one of the most critical aspects of the whole analysis and probably the major source of systematical uncertainties. For small $\Delta\Gamma_s$ and \mathcal{A}^Δ , neglecting the proper time resolution and using the oversimplified representation of the proper time acceptance function as the linear function $\epsilon(\tau) = \epsilon_0(1 + \epsilon_1\tau)$, one gets the observed distribution for signal events as function of the dimensionless variable $t' = \Gamma_s t$:

$$\frac{d}{dt'} \mathcal{N}_{B_s^0 \rightarrow \phi \mathcal{P} \gamma} \propto e^{-t'} \left[1 - \left\{ \mathcal{A}^\Delta \left(\frac{\Delta\Gamma_s}{2\Gamma_s} \right) + \epsilon_1 \right\} t' + \frac{1}{2} \left(\frac{\Delta\Gamma_s}{2\Gamma_s} \right)^2 (t')^2 + \dots \right].$$

Using the estimate of $\frac{\Delta\Gamma_s}{\Gamma_s} \approx 0.12$, one obtains that to achieve an acceptance related uncertainty $\sigma(\mathcal{A}^\Delta) \sim 0.1$, which corresponds to half of the expected statistical precision for 2 fb^{-1} of accumulated data, one needs to know the slope of the proper time acceptance function with a precision of $0.006 \times \Gamma_s$.

Three methods to extract the acceptance function $\epsilon_{B_s^0 \rightarrow \phi \gamma}(\tau)$ for $B_s^0 \rightarrow \phi \gamma$ decay from the data are proposed. One can extract the proper time acceptance function using either the calibration channel $B^0 \rightarrow K^{*0} \gamma$ or the calibration channel $B_s^0 \rightarrow \phi J/\psi$. Note here that

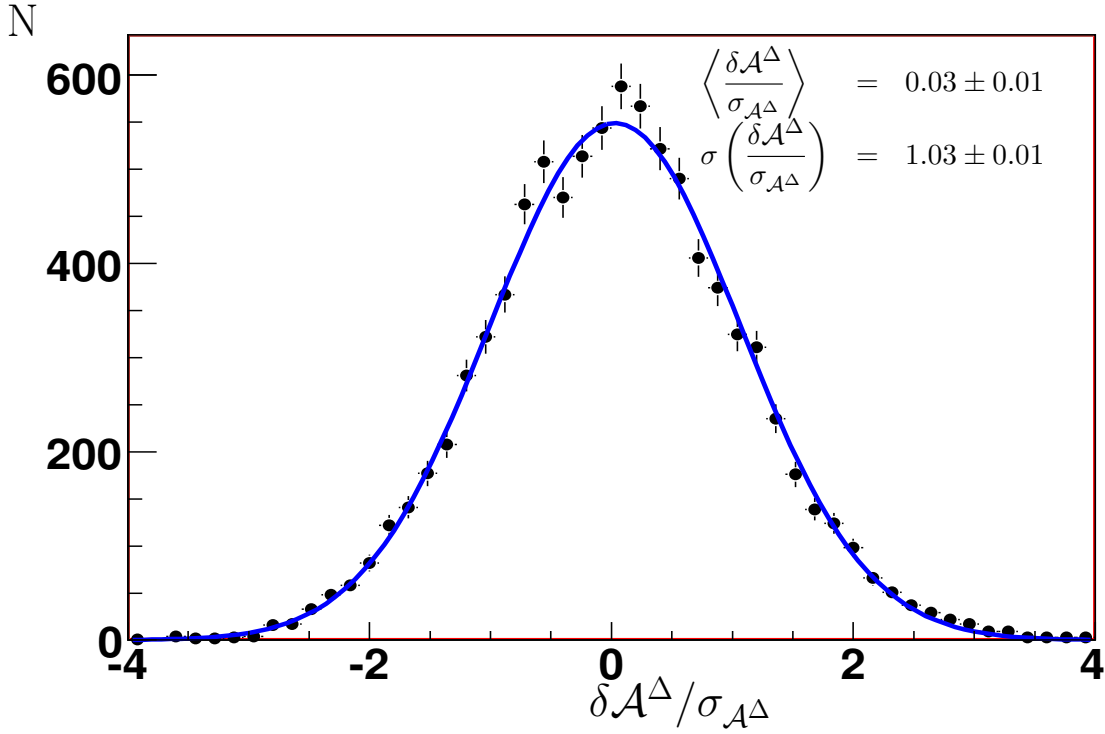


Figure 12: The pull distributions of \mathcal{A}^Δ for $\mathcal{O}(10^4)$ toy experiments. The curve shows a Gaussian fit, with mean value 0.03 ± 0.01 and width 1.03 ± 0.01 .

to achieve the desired statistical precision in the knowledge of the proper time acceptance function, only calibration channels with large event yields can be used. Alternatively to the proposed calibration channels the proper time acceptance function can be extracted per event using a “lifetime swimming” method.

Extraction of proper time acceptance using $B^0 \rightarrow K^{*0}\gamma$ decays

The first method relies on the fact that for $B^0 \rightarrow (K^{*0} \rightarrow K^+\pi^-)\gamma$ the theoretical lifetime distribution is simple and well known. For these decays the shape of the proper time acceptance function can easily be extracted from the measured proper time distribution. For 7×10^4 reconstructed $B^0 \rightarrow K^{*0}\gamma$ events, neglecting backgrounds, the parameters for the acceptance function $\epsilon_{B^0 \rightarrow K^{*0}\gamma}(\tau)$ in Eq. (3.3) can be determined with the following precision:

$$\begin{aligned}\sigma_a &= 0.01 \\ \sigma_c &= 0.02 \quad .\end{aligned}$$

It has been shown that a bias $\delta a = 0.04$ in the parameter a translates into a shift of the observed value of \mathcal{A}^Δ , $\delta \mathcal{A}^\Delta \sim 0.2$. Under the assumption that the shape of the proper time acceptance function is the same for $B_s^0 \rightarrow \phi\gamma$ and $B^0 \rightarrow K^{*0}\gamma$ this method provides

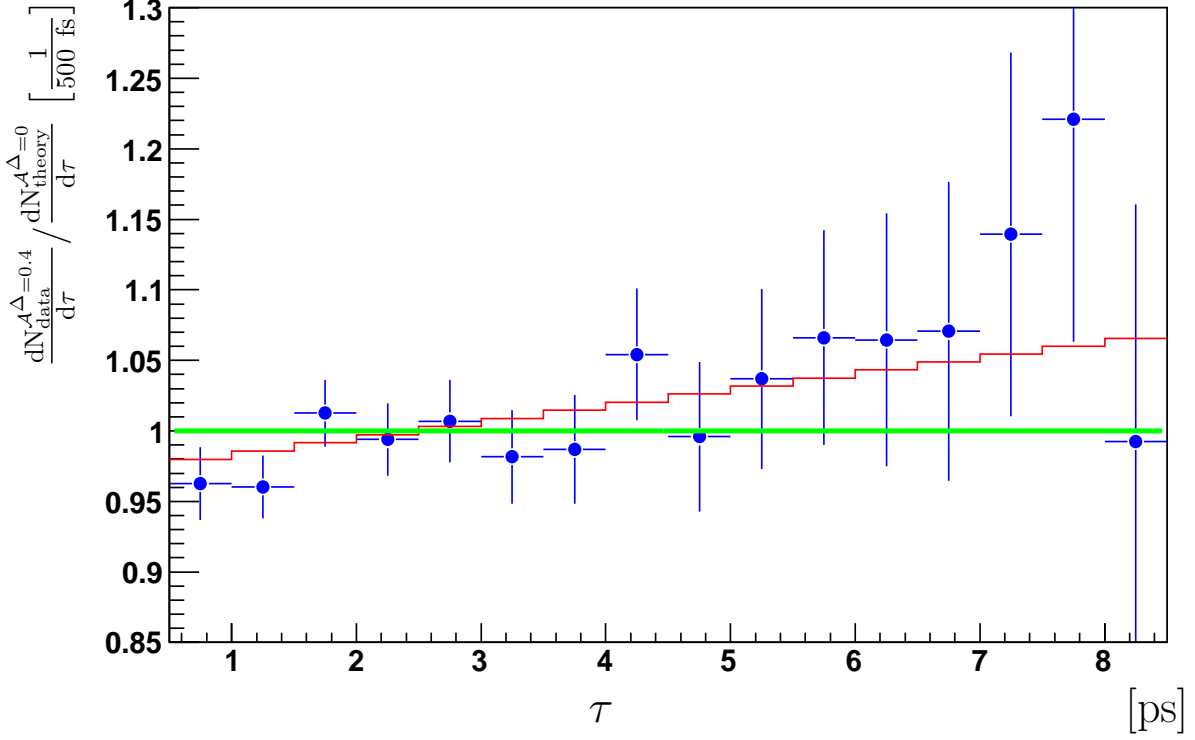


Figure 13: The ratio of Monte Carlo data for $B_s^0 \rightarrow \phi\gamma$, simulated with $\mathcal{A}^\Delta = 0.4$, to the theory expectation for $\mathcal{A}^\Delta = 0$, as a function of the B_s^0 proper lifetime for a toy experiment equivalent to 2 fb^{-1} of accumulated data. The red histogram indicates the expected dependence.

an adequate statistical precision for the determination of the proper time acceptance function. The systematic uncertainty in \mathcal{A}^Δ related to the statistical errors of the above acceptance parameters corresponds to a quarter of the expected statistical error of \mathcal{A}^Δ for a nominal year of data taking.

The off-line and HLT selection criteria for $B_s^0 \rightarrow \phi\gamma$ and $B^0 \rightarrow K^{*0}\gamma$ events are very similar, and the L0 trigger condition are identical. However, due to the small energy release in the decay $\phi \rightarrow K^+K^-$ the vertex resolution for $B_s^0 \rightarrow \phi\gamma$ events is significantly worse than for $B^0 \rightarrow K^{*0}\gamma$ events, resulting in a difference in the proper time acceptance for both channels. A Monte Carlo study with large samples of $B_s^0 \rightarrow \phi\gamma$ and $B^0 \rightarrow K^{*0}\gamma$ clearly exhibits this difference:

$$\left. \begin{array}{l} a = 0.84 \pm 0.04 \text{ ps}^{-1} \\ c = 2.16 \pm 0.08 \end{array} \right\} \text{ for } B_s^0 \rightarrow \phi\gamma \quad (3.7a)$$

$$\left. \begin{array}{l} a = 1.00 \pm 0.04 \text{ ps}^{-1} \\ c = 2.20 \pm 0.09 \end{array} \right\} \text{ for } B^0 \rightarrow K^{*0}\gamma \quad (3.7b)$$

Here the uncertainties are statistical only. The Monte Carlo samples used for this

comparison are a factor 6(30) smaller than the the yield expected for data for the $B_s^0 \rightarrow \phi\gamma(B^0 \rightarrow K^{*0}\gamma)$ channel correspondingly.

One clearly observes a significant difference in the parameter a . Without taking this difference into account one would get a large bias in the measurement of \mathcal{A}^Δ . A proper re-weighting of the $B^0 \rightarrow K^{*0}\gamma$ events relying on Monte Carlo can be used to correct the difference.

Extraction of proper time acceptance using “lifetime swimming” acceptance

A method to evaluate the per-event acceptance as a function of proper decay time by sliding the decay tree along the B flight direction is under investigation. For a given $B_{(s)}$ decay, the whole decay tree is moved along the $B_{(s)}$ flight direction, leaving the $B_{(s)}$ decay kinematics unchanged.

The effect on the proper time acceptance of an impact parameter cut on any final state particle or a cut on the $B_{(s)}$ -meson direction angle can be evaluated event by event¹¹. This method has been used by CDF to measure the B^+ lifetime in the decay mode $B^+ \rightarrow D^0\pi^+$ [61]. Its application by LHCb for the measurement of the B_d lifetime in $B_d \rightarrow D^-\pi^+$ decays is described in Ref. [62].

As a proof of principle, this idea has also been applied to the decay mode $B^0 \rightarrow K^{*0}\gamma$. Fully simulated $B^0 \rightarrow K^{*0}\gamma$ events have been reconstructed using standard LHCb software and selected using particle identification, vertex information and invariant masses. In addition, the impact parameters of kaons and pions are required to be above 0.1 mm. The B direction angle is required to be less than 0.05 mrad. The last two requirements are expected to distort the proper time distribution. The before-acceptance proper time distribution, which is an exponential function convoluted by a resolution function, is assumed to be known. The proper time distribution for signal events is shown by the open histogram in Figure 14. Superimposed is the sum of the normalized per event probability density functions (pdf) of proper time, which is the product of the known before-acceptance proper time distribution and the per-event acceptance function. As expected, the two distributions match very well.

This demonstrates that the per-event pdf defined in this way is a good description of the proper time distribution and can be directly used in maximum likelihood fitting for the extraction of physical parameters.

Alternatively, we can evaluate the average acceptance function by dividing the sum of the per-event pdfs by the before-acceptance proper time distribution. Figure 15 shows the average acceptance functions estimated using truth information and using the per-event acceptance method. The ratio between them is shown in Figure 16, which shows no dependence on proper time above 0.3 ps.

While these preliminary results are encouraging, more work is needed to get this method to work for $B \rightarrow V\gamma$. In particular we need to understand how to use this method in the presence of background.

¹¹ The $B_{(s)}$ direction angle variable is defined as the angle between the the $B_{(s)}$ reconstructed momentum and the $B_{(s)}$ flight direction, evaluated as the vector from the primary vertex to the $B_{(s)}$ decay vertex.

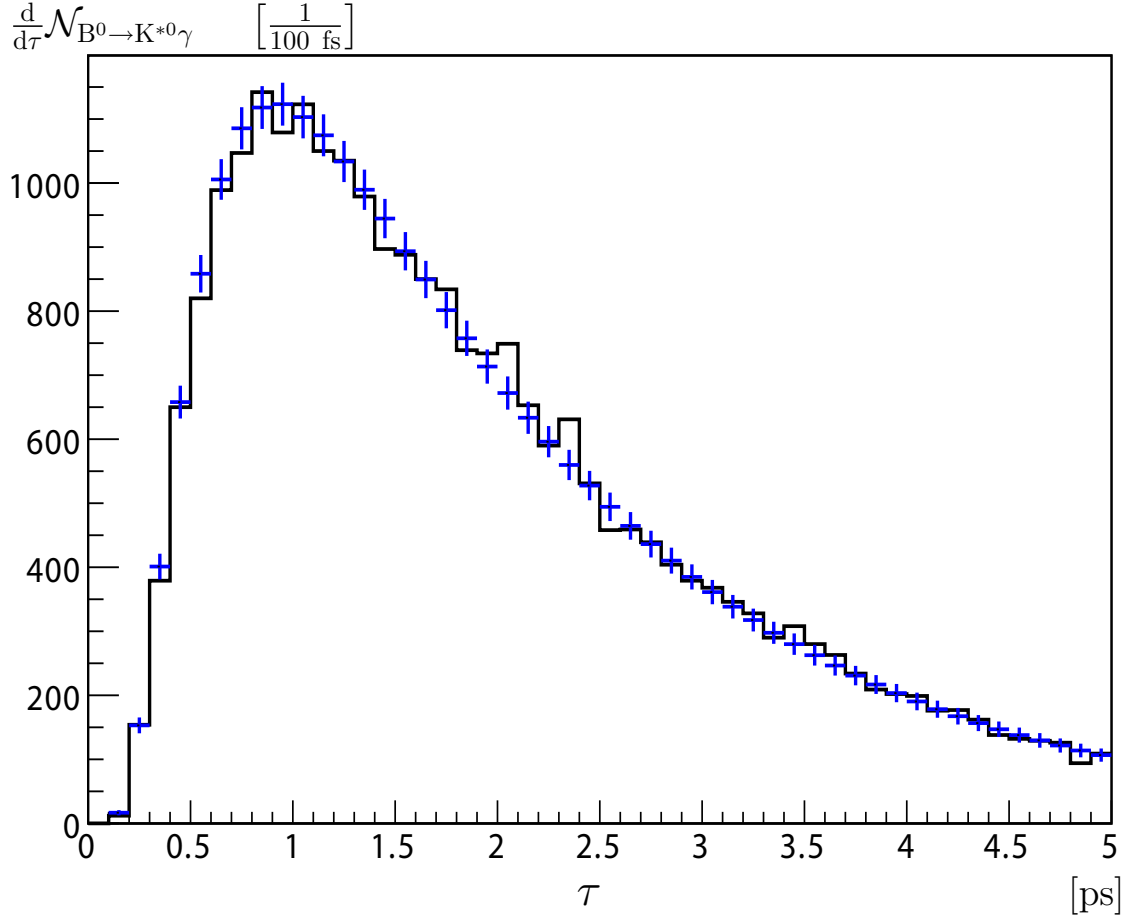


Figure 14: The proper time distribution of signal events $B^0 \rightarrow K^{*0}\gamma$ (open histogram), superimposed with the sum of normalized per event probability density functions (blue histogram with error bars).

Extraction of proper time acceptance function from $B_s^0 \rightarrow \phi J/\psi$ decay

The third approach relies on the possibility of selecting a large sample of *lifetime-unbiased* $B_s^0 \rightarrow \phi J/\psi$ events [10, 63]. If such selection can be done without cuts on the impact parameters of the kaons the events can be used for the determination of the acceptance $\epsilon_{B_s^0 \rightarrow \phi\gamma}(\tau)$. In this case the shape of the proper time acceptance function can be obtained using the relative acceptance of $B_s^0 \rightarrow \phi J/\psi$ events, where one applies the cuts, similar to the selection cuts for $B_s^0 \rightarrow \phi\gamma$ events, to the distribution without such cuts. Clearly one needs to mimic the decay $B_s^0 \rightarrow \phi\gamma$ as close as possible, and it is necessary to use B_s vertices reconstructed from dikaon system only. Cuts on the B_s -vertex quality, direction angle, χ^2 of the lifetime fit and other cuts need to be applied with respect to this “fake” B_s vertex for the “lifetime-unbiased” selected $B_s^0 \rightarrow \phi J/\psi$ events. Using this technique one can obtain the relative (with respect to the *lifetime-unbiased* selection) $\epsilon_{B_s^0 \rightarrow \phi J/\psi}(\tau)$. E.g. applying the cut on the direction angle of B_s , one can evaluate its acceptance, as

$$\epsilon_{B^0 \rightarrow K^*0\gamma}(\tau)$$

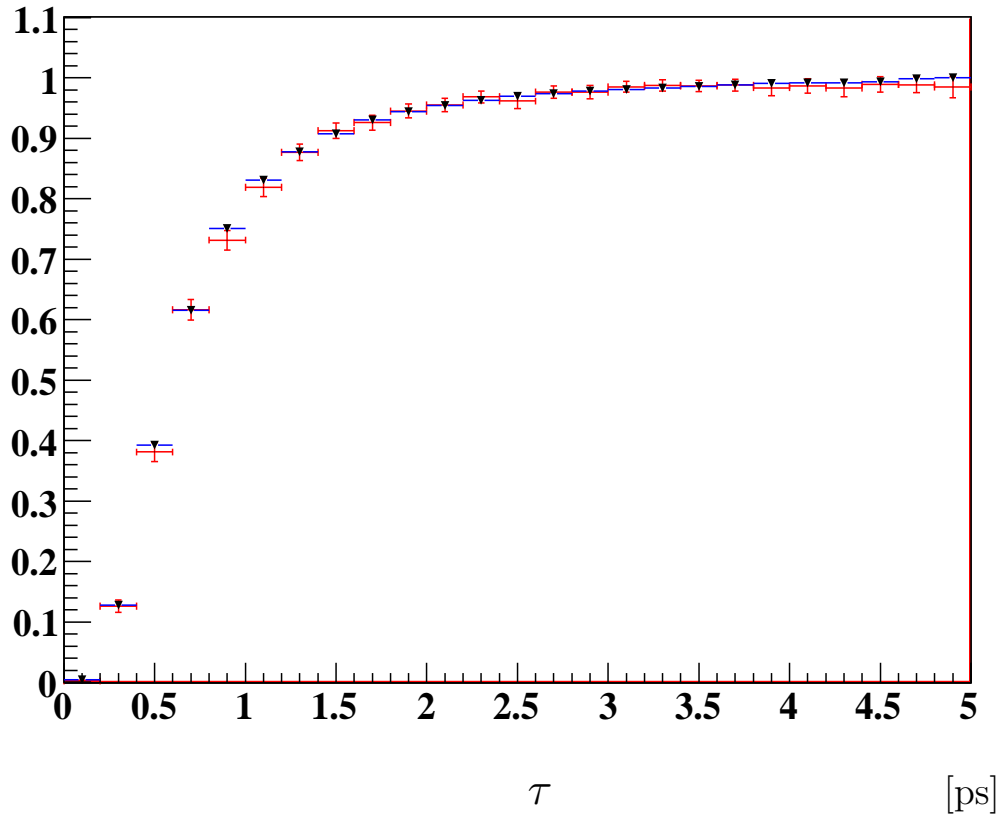


Figure 15: The proper time acceptance functions determined using Monte Carlo truth information $\epsilon_{B^0 \rightarrow K^*0\gamma}^{MC}(\tau)$ (red crosses) and “per-event-acceptance” method $\epsilon_{B^0 \rightarrow K^*0\gamma}^{acc}(\tau)$ (black triangles with blue error bars).

shown in Figure 17.

Due to the difference in the event kinematics, triggering, reconstruction and identification of $J/\psi \rightarrow \mu^+\mu^-$ with respect to energetic photon in $B_s^0 \rightarrow \phi\gamma$, the acceptances $\epsilon_{B_s^0 \rightarrow \phi J/\psi}(\tau)$ and $\epsilon_{B_s^0 \rightarrow \phi\gamma}(\tau)$ will be different. However, we hope that with the proper re-weighting of $B_s^0 \rightarrow \phi J/\psi$ events one could obtain a re-weighted acceptance function $\epsilon_{B_s^0 \rightarrow \phi J/\psi}^*(\tau)$ for which the ratio of lifetime acceptance functions $r_\epsilon(\tau)$, defined as

$$r_\epsilon(\tau) \equiv \frac{\epsilon_{B_s^0 \rightarrow \phi\gamma}(\tau)}{\epsilon_{B_s^0 \rightarrow \phi J/\psi}^*(\tau)} \quad (3.8)$$

is constant.

The available Monte Carlo event samples of $B_s^0 \rightarrow \phi\gamma$ and $B_s^0 \rightarrow \phi J/\psi$ events are limited and do not allow to prove or disprove this hypothesis. To get a feeling of the validity of this procedure the available event statistics were increased by releasing all but one selection cut.

$$\epsilon_{B^0 \rightarrow K^*0\gamma}^{\text{MC}}(\tau) / \epsilon_{B^0 \rightarrow K^*0\gamma}^{\text{acc}}(\tau)$$

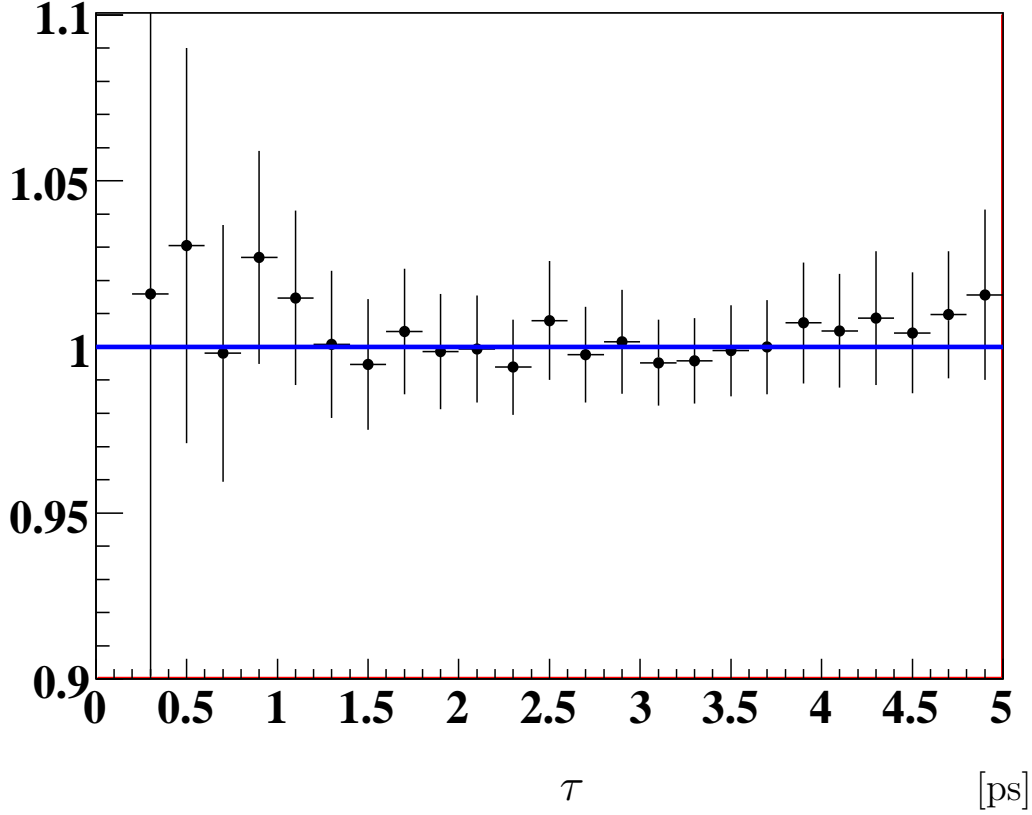


Figure 16: The ratio of proper time acceptance functions determined using Monte Carlo truth information $\epsilon_{B^0 \rightarrow K^*0\gamma}^{\text{MC}}(\tau)$ and the “per-event-acceptance” method $\epsilon_{B^0 \rightarrow K^*0\gamma}^{\text{acc}}(\tau)$.

The cuts with the largest effect on the proper time acceptance are the cut on the minimum χ_{IP}^2 of impact parameter of the kaon with respect to the primary vertex, and the cut on the angle between the B_s momentum and the flight direction, evaluated as the vector from the primary vertex to the B_s decay vertex.

Figure 18 shows the ratio of proper time acceptance functions $r_\epsilon(\tau)$ in the case one applies the cut on the direction angle of the B_s candidate. The minimal value of χ_{IP}^2 of impact parameter for the kaons have been used as re-weighting function. After the re-weighting the ratio of proper time acceptance function has only a modest dependence on the proper time for for $c\tau > 200 \mu\text{m}$.

The usage of the decay angle of B_s as a re-weighting variable allows to decrease the dependence of the ratio $r_\epsilon(\tau)$ on the proper time when a cut on the minimum value of χ_{IP}^2 value of the impact parameter of kaons is applied, as shown in Figure 19. The ratio of proper time acceptance functions $r_\epsilon(\tau)$ is practically independent of the proper time for $c\tau > 200 \mu\text{m}$ within the statistical precision of the available Monte Carlo samples. For further studies the available Monte Carlo samples of $B_s^0 \rightarrow \phi\gamma$ would need to be increased

$\epsilon_{B_s^0 \rightarrow \phi J/\psi}(\tau)$ [a.u.]

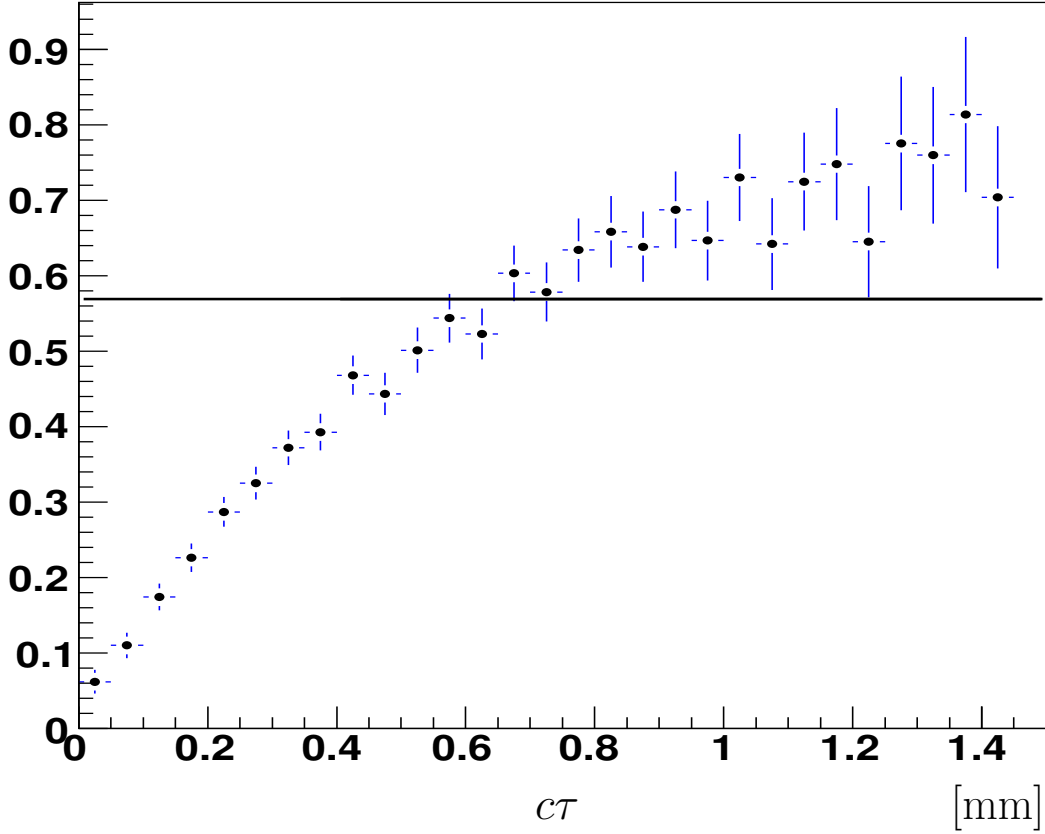


Figure 17: The relative lifetime acceptance function $\epsilon_{B_s^0 \rightarrow \phi J/\psi}(\tau)$ for an applied cut on the direction angle of B_s -meson.

by a factor of 30 to reach the statistics equivalent to 2 fb^{-1} of integrated luminosity.

It is possible that the combination of these re-weighting functions will eliminate all dependencies. However currently available samples of Monte Carlo events do not allow to estimate the precision of this method.

Study of the proper time resolution and the possible proper time biases

The technique of “fake” B_s -vertex reconstruction also allows to determine or calibrate the proper time resolution by comparison of the proper time determined for $B_s^0 \rightarrow \phi J/\psi$ events using the regular four-prong B_s^0 vertex and “fake” two-prong B_s^0 vertex. The difference is dominated by resolution in the reconstruction of the $\phi \rightarrow K^+K^-$ decay vertex. The possible biases in the determination of the proper lifetime also can be checked using this technique.

The effect of uncertainties of Γ_s or $\Delta\Gamma_s$ on the measurement of \mathcal{A}^Δ has been studied using toy simulations corresponding to a scenario with $\Gamma_s = 0.6993$, $\Delta\Gamma_s = 0.084$ and

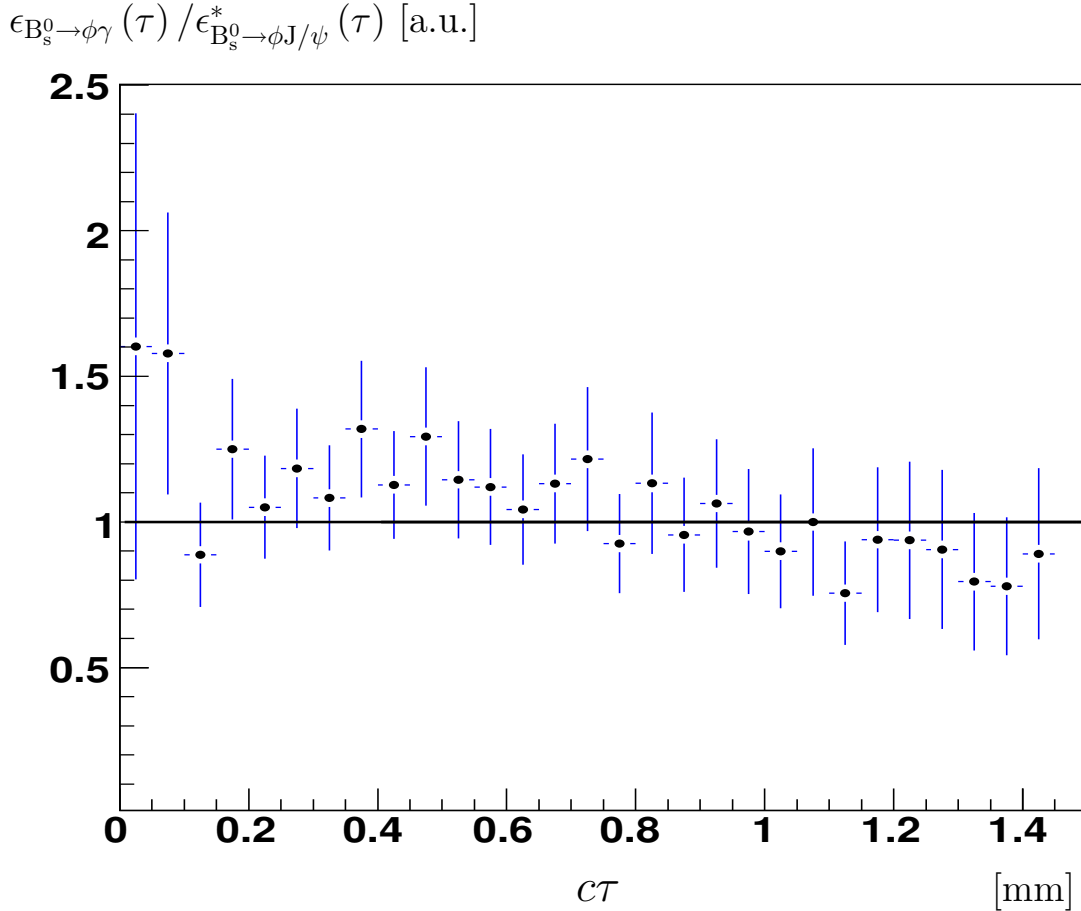


Figure 18: The ratio of lifetime acceptance functions $r_\epsilon(\tau)$ when a cut has been made on the direction angle, after re-weighting of $B_s^0 \rightarrow \phi J/\psi$ events with χ_{IP}^2 .

$\mathcal{A}^\Delta = 0.5$. The study shows that a relative shift of the value Γ_s by 0.5% leads to a shift in \mathcal{A}^Δ by 0.2, independent of the value of \mathcal{A}^Δ . If $\frac{\Delta\Gamma_s}{\Gamma_s}$ will be under-estimated by 10% (relative) \mathcal{A}^Δ will be over-estimated by 18%. If $\frac{\Delta\Gamma_s}{\Gamma_s}$ will be over-estimated by 10% (relative) \mathcal{A}^Δ will be under-estimated by 13%.

We will use the values of Γ_s and $\frac{\Delta\Gamma_s}{\Gamma_s}$ measured at LHCb for the $B_s^0 \rightarrow \phi J/\psi$ decays, where these parameters will be measured with very small statistical error. It is expected that some of the systematic effects, such as wrong magnetic field, will affect $B_s^0 \rightarrow \phi J/\psi$ and $B_s^0 \rightarrow \phi\gamma$ in a similar way, therefore the bias in \mathcal{A}^Δ may be small if one uses the experimentally determined $B_s^0 \rightarrow \phi J/\psi$ lifetime even if it is significantly shifted compared to the true value. Other systematic effects, such as misalignment and proper time acceptance, may not completely cancel in the two decay modes for the measurement of \mathcal{A}^Δ . This will be the subject of future studies.

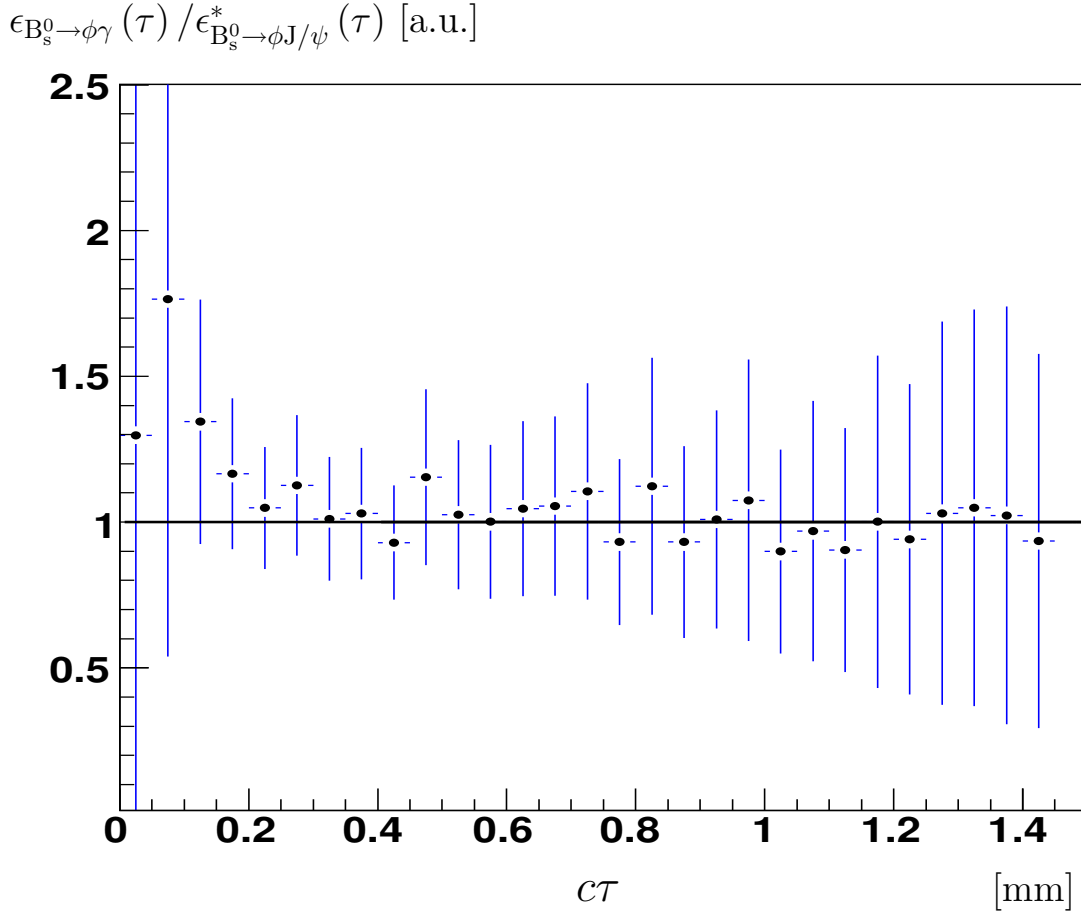


Figure 19: The ratio of lifetime acceptance functions $r_\epsilon(\tau)$ when a cut is applied on χ_{IP}^2 for kaons, after re-weighting of $B_s^0 \rightarrow \phi J/\psi$ events with the decay angle of B_s -meson.

The alternative selection of $B_s^0 \rightarrow \phi\gamma$

In order to minimize the systematic error related to the parameterization of the proper time acceptance function an alternative selection of $B_s^0 \rightarrow \phi\gamma$ events is under study. It is possible to replace the cut on the direction angle of the B_s^0 -candidate with a cut on the reconstructed lifetime of the B_s^0 -candidate. Such a selection allows to obtain a “step-like” shape of the proper time acceptance. Using such a selection one can achieve, for a well chosen value of the cut, the same efficiency for the signal events and the same suppression of minimum-bias background as the standard selection. Moreover with this approach one removes from the analysis the problematic area of small proper lifetimes, which causes problem for methods described above, see Figures 16 and 19. In addition it has been demonstrated that an HLT2 trigger selection without explicit cuts on the impact parameters of kaons is possible. However currently is not possible to check the performance of such a selection against the major expected background from $b\bar{b}$ -events.

The strategy for the proper time acceptance function

All three methods described above will be used for the extraction of the proper time acceptance function, allowing to evaluate the systematic error.

Assuming that one can extract the actual proper time acceptance function for $B^0 \rightarrow K^{*0}\gamma$ or $B_s^0 \rightarrow \phi\gamma$ decays, different strategies for the use of this information are under consideration now. The actual strategy adopted will depend on the level of agreement between the shape of the acceptance function extracted for the calibration channel and the shape of the acceptance function expected from Monte Carlo simulation. In the case of good agreement one gets confidence in Monte Carlo simulation and in the predicted shape of the acceptance function for $B_s^0 \rightarrow \phi\gamma$ events. For the fit of the $B_s^0 \rightarrow \phi\gamma$ data one could, in this case, use the shape obtained from the Monte Carlo analysis. In the case of some discrepancy between the the shapes obtained from the Monte Carlo data and from the calibration channels the strategy could be twofold. First, obviously, one can try to tune the Monte Carlo simulation to reproduce the acceptance functions obtained for the calibration channels. Alternatively one can assume that the Monte Carlo simulation still reproduces reasonably the *ratio* of acceptance functions and one can use this hypothesis in the overall fit. Using the calibration channel $B^0 \rightarrow K^{*0}\gamma$ one can perform a common fit for the $B^0 \rightarrow K^{*0}\gamma$ and $B_s^0 \rightarrow \phi\gamma$ events and keep the parameters describing the shape of the acceptance function for $B^0 \rightarrow K^{*0}\gamma$ events free in the fit, while one fixes the shape of the ratio between the acceptance functions for $B_s^0 \rightarrow \phi\gamma$ and $B^0 \rightarrow K^{*0}\gamma$ decay modes from Monte Carlo simulation. The evaluation of the systematic errors and a possible bias requires special studies. The comparison of the result obtained by the first and second approaches will provide an estimate for the systematic error associated to the shape of the acceptance functions.

4 The early measurements

The early measurements are those that can be done with low integrated luminosity, significantly less than 2 fb^{-1} . In this section we discuss measurements with 10 pb^{-1} , 100 pb^{-1} and 500 pb^{-1} . The expected yields are summarized in Table 9.

Table 9: The expected yields for data samples of 10 pb^{-1} , 100 pb^{-1} and 500 pb^{-1} of integrated luminosity.

Decay Mode	10 pb^{-1}	100 pb^{-1}	500 pb^{-1}
$B^0 \rightarrow K^{*0} \gamma$	370	4×10^3	2×10^4
$B_s^0 \rightarrow \phi \gamma$	55	550	3×10^3
$B^+ \rightarrow \phi K^+ \gamma$	35	350	2×10^3
$\Lambda_b \rightarrow \Lambda^0 \gamma$			200
$\Lambda_b \rightarrow \Lambda^0(1520) \gamma$		250	1.1×10^3
$\Lambda_b \rightarrow \Lambda^0(1670) \gamma$		130	650
$\Lambda_b \rightarrow \Lambda^0(1690) \gamma$		130	650

These estimates are obtained using a downscaling from 2 fb^{-1} , see Table 1, and assuming the nominal detector conditions and no inefficiency from the High Level Trigger (HLT). The numbers are probably optimistic, as there may be imperfections for early data, such as:

1. HLT (including HLT1 and HLT2) inefficiencies;
2. track reconstruction inefficiencies, and worsening of spatial or momentum resolution;
3. the absence or poorer hadron identification with RICH detectors;
4. inefficiency of calorimeter cells due to dead, masked and noisy channels;
5. imperfect calibration of calorimeter channels.

The effect of some of these points will be considered below.

4.1 The studies with 10 pb^{-1}

The number of detected signal events are summarized in the second column of Table 9. The study of background composition for $B^0 \rightarrow K^{*0} \gamma$ and $B_s^0 \rightarrow \phi \gamma$ [2] shows that the background estimate is rather stable with respect to worse hadron identification - at most a doubling of the background level could be expected. The calorimeter commissioning is progressing well, and much less than 2% of dead, noisy and masked cells in the calorimeters are expected. Using the estimates for the $B^0 \rightarrow K^{*0} \gamma$ decay, one can see that under the assumption that the L0 trigger [9] is operating properly, one can observe the $B^0 \rightarrow K^{*0} \gamma$ signal, even in the case of all conservative estimates. Even if the calorimeter is

miscalibrated up to 5%, which would correspond to an increase of the background level by a factor ~ 2 , see Appendix C and Figure 20, the $B^0 \rightarrow K^{*0}\gamma$ signal should still be clearly visible. The position of the signal peak could in principle allow to estimate the global miscalibration factor for photons of very high energy, and the width will allow to estimate the channel to channel calorimeter miscalibration. Due to lower statistics the visibility of $B_s^0 \rightarrow \phi\gamma$ and $B^+ \rightarrow \phi K^+\gamma$ signals will not be evident. In summary one can conclude that with 10 pb^{-1} of integrated luminosity, one should be able to see a $B^0 \rightarrow K^{*0}\gamma$ peak even in rather pessimistic scenarios.

4.2 The measurements with 100 pb^{-1}

The number of detected signal events are summarized in the third column of Table 9. With such an event statistics one can safely assume that the calorimeter (at least Ecal) is calibrated at the level of 1–1.5 %, and that the high energy calibration is also validated, see Appendix C.

We should be able to see $B_s^0 \rightarrow \phi\gamma$ and $B^+ \rightarrow \phi K^+\gamma$ signals. If the background to signal ratio, \mathcal{B}/\mathcal{S} , for $\Lambda_b \rightarrow \Lambda^0(1520)\gamma$, $\Lambda_b \rightarrow \Lambda^0(1670)\gamma$ and $\Lambda_b \rightarrow \Lambda^0(1690)\gamma$ is a somewhat lower compared to the upper limit that has been determined from the limited Monte Carlo statistics [5, 6, 7], than the observation of these channels can be possible¹².

The large statistics of $B^0 \rightarrow K^{*0}\gamma$ events allows us to further check and validate the calorimeter calibration at high energy, and to split the calorimeter into several regions to check the global miscalibration coefficients for these regions.

At this moment one can try to test the algorithms for π^0/γ -separation at very high energy, see Appendix D. Due to large statistics of $B^0 \rightarrow K^{*0}\gamma$ events the optimization of the algorithm could be performed using real data¹³, directly analysing the behaviour of signal and background.

The direct \mathcal{CP} -asymmetry for $B^0 \rightarrow K^{*0}\gamma$

With accumulated statistics around 100 fb^{-1} one can make the measurement of the direct \mathcal{CP} asymmetry for the $B^0 \rightarrow K^{*0}\gamma$ decay mode. The straightforward determination of this asymmetry is limited by the unknown or badly measured detector and production asymmetries. However using the calibration channel $B^0 \rightarrow K^{*0}J/\psi$, one can build the ratios \mathcal{R} and $\bar{\mathcal{R}}$:

$$\mathcal{R} = \frac{\mathcal{N}_{B^0 \rightarrow K^{*0}\gamma}}{\mathcal{N}_{B^0 \rightarrow K^{*0}J/\psi}} \quad (4.1a)$$

$$\bar{\mathcal{R}} = \frac{\mathcal{N}_{\bar{B}^0 \rightarrow \bar{K}^{*0}\gamma}}{\mathcal{N}_{\bar{B}^0 \rightarrow \bar{K}^{*0}J/\psi}} \quad (4.1b)$$

¹²In general for these channels the background conditions are expected to be similar to the $B^0 \rightarrow K^{*0}\gamma$ mode.

¹³Note here that we do not need to know the exact value of the background suppression factor from this algorithm, we just need to know the signal efficiency.

From these ratios one can construct the asymmetry $\mathcal{A}_{\mathcal{R}}$:

$$\mathcal{A}_{\mathcal{R}} = \frac{\bar{\mathcal{R}} - \mathcal{R}}{\bar{\mathcal{R}} + \mathcal{R}}. \quad (4.2)$$

Clearly the production asymmetries and, to first order, the detector asymmetries cancel in the asymmetry $\mathcal{A}_{\mathcal{R}}$. As a result the asymmetry $\mathcal{A}_{\mathcal{R}}$ is a function of the direct \mathcal{CP} asymmetries $\mathcal{A}_{K^*0\gamma}^{\text{dir}}$ and $\mathcal{A}_{K^*0J/\psi}^{\text{dir}}$ only¹⁴:

$$\mathcal{A}_{\mathcal{R}} = \frac{\mathcal{A}_{K^*0\gamma}^{\text{dir}} - \mathcal{A}_{K^*0J/\psi}^{\text{dir}}}{1 - \mathcal{A}_{K^*0\gamma}^{\text{dir}} \mathcal{A}_{K^*0J/\psi}^{\text{dir}}}, \quad (4.3)$$

where the direct \mathcal{CP} -asymmetries $\mathcal{A}_{K^*0\gamma}^{\text{dir}}$ and $\mathcal{A}_{K^*0J/\psi}^{\text{dir}}$ are defined as:

$$\mathcal{A}_{K^*0\gamma}^{\text{dir}} = \frac{\mathcal{B}_{\bar{B}^0 \rightarrow \bar{K}^*0\gamma} - \mathcal{B}_{B^0 \rightarrow K^*0\gamma}}{\mathcal{B}_{\bar{B}^0 \rightarrow \bar{K}^*0\gamma} + \mathcal{B}_{B^0 \rightarrow K^*0\gamma}} \quad (4.4a)$$

$$\mathcal{A}_{K^*0J/\psi}^{\text{dir}} = \frac{\mathcal{B}_{\bar{B}^0 \rightarrow \bar{K}^*0J/\psi} - \mathcal{B}_{B^0 \rightarrow K^*0J/\psi}}{\mathcal{B}_{\bar{B}^0 \rightarrow \bar{K}^*0J/\psi} + \mathcal{B}_{B^0 \rightarrow K^*0J/\psi}}. \quad (4.4b)$$

The cancellation of reconstruction asymmetries from $\mathcal{A}_{\mathcal{R}}$ is exact if the selection criteria used for the $B^0 \rightarrow K^*0\gamma$ and the $B^0 \rightarrow K^*0J/\psi$ selection do not result in a significant difference in the phase space for the important variables, or the reconstruction efficiency is constant. Otherwise the necessary corrections are of the order $\left(\mathcal{A}_{K^*0\gamma}^{\text{rec}} - \mathcal{A}_{K^*0J/\psi}^{\text{rec}}\right)$,

and clearly do not exceed $\frac{\int \varepsilon(\Phi) (p^s(\Phi) - p^c(\Phi)) d\Phi}{\int \varepsilon(\Phi) (p^s(\Phi) + p^c(\Phi)) d\Phi}$, where $\varepsilon(\Phi)$ is the reconstruction efficiency, $p^s(\Phi)$ and $p^c(\Phi)$ are probability distribution functions for the signal and calibration channel. These corrections can be estimated from Monte Carlo simulation. If they appear to be the limiting factors, the phase space can be subdivided into a few bins and the measurement of $\mathcal{A}_{\mathcal{R}}$ can be performed independently in each bin, and the results from the different bins can be averaged.

¹⁴ The exact expression is:

$$\mathcal{A}_{\mathcal{R}} = \frac{\left(\mathcal{A}_{K^*0\gamma}^{\text{dir}} - \mathcal{A}_{K^*0J/\psi}^{\text{dir}}\right) + \left(\mathcal{A}_{K^*0\gamma}^{\text{rec}} - \mathcal{A}_{K^*0J/\psi}^{\text{rec}}\right)}{1 + \left(\mathcal{A}_{K^*0\gamma}^{\text{dir}} - \mathcal{A}_{K^*0J/\psi}^{\text{dir}}\right) \left(\mathcal{A}_{K^*0\gamma}^{\text{rec}} - \mathcal{A}_{K^*0J/\psi}^{\text{rec}}\right) - \mathcal{A}_{K^*0\gamma}^{\text{dir}} \mathcal{A}_{K^*0J/\psi}^{\text{dir}} - \mathcal{A}_{K^*0\gamma}^{\text{rec}} \mathcal{A}_{K^*0J/\psi}^{\text{rec}}},$$

where the detector asymmetries $\mathcal{A}_{K^*0\gamma}^{\text{rec}}$ and $\mathcal{A}_{K^*0J/\psi}^{\text{rec}}$ are defined as:

$$\mathcal{A}_{K^*0\gamma}^{\text{rec}} = \frac{\varepsilon_{\bar{B}^0 \rightarrow \bar{K}^*0\gamma} - \varepsilon_{B^0 \rightarrow K^*0\gamma}}{\varepsilon_{\bar{B}^0 \rightarrow \bar{K}^*0\gamma} + \varepsilon_{B^0 \rightarrow K^*0\gamma}}$$

$$\mathcal{A}_{K^*0J/\psi}^{\text{rec}} = \frac{\varepsilon_{\bar{B}^0 \rightarrow \bar{K}^*0J/\psi} - \varepsilon_{B^0 \rightarrow K^*0J/\psi}}{\varepsilon_{\bar{B}^0 \rightarrow \bar{K}^*0J/\psi} + \varepsilon_{B^0 \rightarrow K^*0J/\psi}}.$$

One gets the explicit expression for $\mathcal{A}_{K^*0\gamma}^{\text{dir}}$:

$$\mathcal{A}_{K^*0\gamma}^{\text{dir}} = \frac{\mathcal{A}_{\mathcal{R}} + \mathcal{A}_{K^*0J/\psi}^{\text{dir}}}{1 + \mathcal{A}_{\mathcal{R}}\mathcal{A}_{K^*0J/\psi}^{\text{dir}}}. \quad (4.5)$$

The asymmetry $\mathcal{A}_{\mathcal{R}}$ could be measured with a statistical precision of 0.018 for 100 pb⁻¹ of data due to the large statistics of $B^0 \rightarrow K^*0\gamma$ and $B^0 \rightarrow K^*0J/\psi$ events. The latter will be selected for calibration and normalization of other interesting decays of B hadrons [10, 11]. The systematic error is expected to be rather small. As a result the final error on $\mathcal{A}_{K^*0\gamma}^{\text{dir}}$ will be dominated by the knowledge of $\mathcal{A}_{K^*0J/\psi}^{\text{dir}}$ from the B factories. It should be possible to measure the $\mathcal{A}_{K^*0\gamma}^{\text{dir}}$ with a precision which is better than the current combined precision from the B factories, $\sigma(\mathcal{A}_{K^*0\gamma}^{\text{dir}}) = 0.028$ [51].

The ratio of $B_s^0 \rightarrow \phi\gamma$ to $B^0 \rightarrow K^*0\gamma$ rates

Another interesting measurement could be the measurement of the ratio of the branching fractions for $B^0 \rightarrow K^*0\gamma$ and $B_s^0 \rightarrow \phi\gamma$. Again, the direct determination of this ratio suffers both from the knowledge of detector and trigger efficiencies and knowledge of the production rates through the ratio of the fragmentation constants f_d/f_s . However using the decay modes $B^0 \rightarrow K^*0J/\psi$ and $B_s^0 \rightarrow \phi J/\psi$ as normalization channels one can make a rather precise measurement of the double ratio $\mathcal{R}^{B_s^0 \rightarrow \phi\gamma}$:

$$\mathcal{R}^{B_s^0 \rightarrow \phi\gamma} = \frac{\mathcal{B}_{B_s^0 \rightarrow \phi\gamma} / \mathcal{B}_{B_s^0 \rightarrow \phi J/\psi}}{\mathcal{B}_{B^0 \rightarrow K^*0\gamma} / \mathcal{B}_{B^0 \rightarrow K^*0J/\psi}} = \frac{\mathcal{B}_{B_s^0 \rightarrow \phi\gamma} / \mathcal{B}_{B^0 \rightarrow K^*0\gamma}}{\mathcal{B}_{B_s^0 \rightarrow \phi J/\psi} / \mathcal{B}_{B^0 \rightarrow K^*0J/\psi}},$$

where again one expects the cancellation of most systematic uncertainties, resulting in a dominantly statistical error of less than 5% for 100 pb⁻¹ of data.

A first look into $B^+ \rightarrow \phi K^+\gamma$ channel

The double ratio technique can be used again to measure, with reduced systematical error, the ratio of branching ratios $B^+ \rightarrow \phi K^+\gamma$ and $B^0 \rightarrow K^*0\gamma$:

$$\mathcal{R}_{\mathcal{D}}^{B^+ \rightarrow \phi K^+\gamma} = \frac{\mathcal{B}_{B^+ \rightarrow \phi K^+\gamma} / \mathcal{B}_{B^0 \rightarrow K^*0\gamma}}{\mathcal{B}_{B^+ \rightarrow K\pi\pi J/\psi} / \mathcal{B}_{B^0 \rightarrow K^*0J/\psi}}.$$

The denominator of this double ratio is well known from the B factories [51]. However in this case not all particle identification efficiencies cancel, therefore additional corrections from Monte Carlo or other calibration channels are required¹⁵. But even in the case of large corrections the measurement could be the most precise determination of the $B^+ \rightarrow \phi K^+\gamma$ branching ratio. Such statistics of $B^+ \rightarrow \phi K^+\gamma$ events will allow a first look to be made

¹⁵Clearly if the the precise measurement of $\mathcal{B}_{B^+ \rightarrow \phi K^+ J/\psi}$ will be available from the B factories, it would be very useful to decrease the systematic uncertainty.

at the Dalitz plots for three-kaon systems separately for the B^+ and B^- cases. Also one can expect the first result on the resonant decomposition and the dominant partial waves. However, the results here depend crucially on the background level.

The clear peak of $B_s^0 \rightarrow \phi\gamma$ decay can be used for investigation of the background in this channel. In particular one needs to compare the proper time distribution in the left and right sidebands, and to check the stability and convergence of 2D fits for proper time versus the reconstructed mass for background events. Clearly the available statistics of background events will be much larger than any possible Monte Carlo event sample, allowing the detailed study of the proper time distributions separately for the left and the right sideband, which is a necessary prerequisite for the background parameterization in the whole 2D plane.

4.3 The measurements with 500 pb⁻¹ and beyond

The number of detected signal events are summarized in the last column of Table 9. Again these numbers do not include the efficiency of the High Level Trigger.

At this moment the calorimeter is assumed to be fully calibrated and understood. The large statistics of $B^0 \rightarrow K^{*0}\gamma$ events will allow this decay mode to be used widely as a normalization channel.

Assuming that with such statistics LHCb will be able to understand the trigger, particle reconstruction and identification, the scaling from Monte Carlo is a good estimate. However, for complicated items, like the flavour tagging, more experience may be required.

With this data set we will be able to commission the algorithm for the π^0/γ -separation at very high energy, see Appendix D. It is assumed that the algorithm has been tested and validated earlier. After the algorithm is commissioned we can expect an overall decrease in the level of background of a factor of 2 [2, 1].

Using 500 pb⁻¹ of data one can perform an unbinned maximum likelihood fit of $B_s^0 \rightarrow \phi\gamma$ events. The expected precision on \mathcal{A}^Δ for the untagged sample is about ~ 0.4 , which is better than any current single measurement from B-factories. However, if the tagged analysis is possible, one can expect to obtain a precision for the measurement of the \mathcal{CP} violating parameters \mathcal{C} and \mathcal{S} of ~ 0.2 .

For the decay channel $B^+ \rightarrow \phi K^+\gamma$, one can start the detailed Dalitz analysis and the partial wave decomposition. In the case of a favourable contribution of partial waves and relative phases interesting results are expected.

If the background to signal ratio, \mathcal{B}/\mathcal{S} , for $\Lambda_b \rightarrow \Lambda^0(1520)\gamma$, $\Lambda_b \rightarrow \Lambda^0(1670)\gamma$ and $\Lambda_b \rightarrow \Lambda^0(1690)\gamma$ is somewhat lower than the upper limit that has been determined from the limited Monte Carlo statistics [5, 6, 7], then the observation of these channels should be possible. The possibility to observe the decay $\Lambda_b \rightarrow \Lambda^0\gamma$ also depends on the status of the High Level Trigger and analysis tools for selection of this challenging mode [5, 6, 7].

With 2 fb⁻¹ of accumulated luminosity the asymmetry \mathcal{A}_R defined by Eq. (4.2) and related to the direct \mathcal{CP} asymmetry $\mathcal{A}_{K^{*0}\gamma}^{\text{dir}}$ (see Eq. (4.3)), could be measured with a statistical precision better than 1% due to the large statistics of $B^0 \rightarrow K^{*0}\gamma$ and $B^0 \rightarrow K^{*0}J/\psi$ events. The systematic error is expected to be rather small due to cancellation

of various systematic asymmetries in the $\mathcal{A}_{\mathcal{R}}$. However, further progress for $\mathcal{A}_{\text{K}^*0\gamma}^{\text{dir}}$ would definitely require more detailed understanding of the systematic uncertainties related to the detector and production asymmetries.

Summary

The basic steps toward the first measurements of radiative B decays in LHCb have been presented. We have concentrated on the probing of photon polarisation in the $\text{B}_s^0 \rightarrow \phi\gamma$ decay. Based on our Monte Carlo simulation for 2 fb^{-1} we expect to reach the uncertainty in the measurement of the parameter \mathcal{A}^Δ , $\sigma_{\mathcal{A}^\Delta} \approx 0.22$. The capability of LHCb experiment to measure this and other parameters has been discussed for different luminosity sets.

The measurement of the direct \mathcal{CP} -asymmetry for $\text{B}^0 \rightarrow \text{K}^*0\gamma$ decay can be performed with statistical precision around 0.018 already with a data-set of an integrated luminosity around 100 pb^{-1} , and the measurements of the ratio of branching fractions for $\text{B}_s^0 \rightarrow \phi\gamma$ and $\text{B}^0 \rightarrow \text{K}^*0\gamma$ can be done with statistical precision less than 5%

Several critical aspects and important prerequisites, like calorimeter calibration, implementation of the HLT, determination of proper time acceptance function from data and γ/π^0 separation at high- E_T have been addressed.

Acknowledgments

We would like to express our gratitude to our colleagues from the LHCb Rare Decays, Calorimeter and Trigger groups. Primarily we thank T. Skwarnicki for opening the door into the world of radiative penguins, A. Bondar, L. Camilleri, B. Delcourt, H. Dijkstra, U. Egede, R. Forty, J. Lefrancois, M. Merk, T. Nakada, N. Nikitin, P. Perret, B. Pietrzyk, G. Raven, M.-H. Schune, S. Stone and U. Uwer for their attention to this work and J. Amoraal, V. Breton, N. Brun, D. Golubkov, Yu. Guz, W. Hulsbergen, P. Koppenburg, G. Lanfranchi, O. Leroy, P. Pakhlov, J. Palacios, C. Parkes, T. du Pree, V. Romanovsky, P. Somogyi, and F. Teubert for the leading contributions, the great help, many useful suggestions and clarifications of various complicated aspects.

Appendix A: Differential B_s^0 decay rates and \mathcal{CP} -violation parameters

The observable rate for $B_s^0 \rightarrow \phi\gamma$ events is:

$$R(t) = \varepsilon^{\text{tag}} \int |A|^2 e^{-\Gamma\tau} \left[\cosh \frac{\Delta\Gamma\tau}{2} - \mathcal{A}^\Delta \sinh \frac{\Delta\Gamma\tau}{2} + (1 - 2\omega)\mathcal{C} \cos \Delta m_s \tau - (1 - 2\omega)\mathcal{S} \sin \Delta m_s \tau \right] \mathcal{K}(\tau, t) d\tau \quad . \quad (\text{A.1a})$$

The observed rate for $\bar{B}_s^0 \rightarrow \phi\gamma$ events is:

$$\bar{R}(t) = \varepsilon^{\text{tag}} \int |A|^2 e^{-\Gamma\tau} \left[\cosh \frac{\Delta\Gamma\tau}{2} - \mathcal{A}^\Delta \sinh \frac{\Delta\Gamma\tau}{2} - (1 - 2\omega)\mathcal{C} \cos \Delta m_s \tau + (1 - 2\omega)\mathcal{S} \sin \Delta m_s \tau \right] \mathcal{K}(\tau, t) d\tau \quad . \quad (\text{A.1b})$$

The rate of untagged events is:

$$R_{no-tag}(t) = (1 - \varepsilon_{tag}) \left(\int |A|^2 e^{-\Gamma\tau} \left[\cosh \frac{\Delta\Gamma\tau}{2} - \mathcal{A}^\Delta \sinh \frac{\Delta\Gamma\tau}{2} \right] \mathcal{K}(\tau, t) d\tau \right) \quad , \quad (\text{A.2})$$

where ε^{tag} is the tagging efficiency, ω is a mistag rate, and the kernel $\mathcal{K}(\tau, t) = \epsilon(t) G(\tau - t)$ is parameterized as the product of the proper time acceptance function $\epsilon(t)$ and the Gaussian resolution function $G(\tau - t)$. The parameters \mathcal{C} , \mathcal{S} and \mathcal{A}^Δ are defined by (1.6). For equations (A.1) it has been assumed that the tagging efficiency for produced B_s and \bar{B}_s mesons are equal, and for equation (A.2) the production asymmetry also has been neglected.

Appendix B: The likelihood function for the $B_s^0 \rightarrow \phi\gamma$ analysis

The probability distribution function (PDF) for the unbinned maximum likelihood fits for $B_s^0 \rightarrow \phi\gamma$ is constructed as follows. For each tagging category κ the PDF can be written as:

$$P_\kappa(t, m) = f_s \frac{1}{\mathcal{N}_S} [e^{-\Gamma\tau} (I_+(\tau) + \kappa(1 - 2\omega)I_-(\tau)) \otimes \mathcal{K}(\tau, t)] \times G_m(m_{\phi\gamma}) + (1 - f_s) \frac{1}{\mathcal{N}_B} f_b(m_{\phi\gamma}, t), \quad (\text{B.1})$$

where f_s is a fraction of signal events, κ can possess three values: $\kappa = -1$ corresponding to B_s , $\kappa = 1$ to \bar{B}_s and $\kappa = 0$ to untagged events, $f_s = \frac{S}{S+B}$ is the signal fraction, the kernel $\mathcal{K}(\tau, t) = \epsilon(t) G(\tau - t)$ is parameterized as the product of the proper time acceptance function $\epsilon(t)$ and the Gaussian resolution function $G(\tau - t)$, $G_m(m_{\phi\gamma})$ is the normalized mass PDF for the signal, which is parameterized by the simple Gaussian, background PDF $f_b(m_{\phi\gamma}, t)$ is defined by (3.4), and the helper functions $I_\pm(\tau)$ and the normalization factors \mathcal{N}_S and \mathcal{N}_B defined as:

$$\begin{aligned} I_+(\tau) &= \cosh \frac{\Delta\Gamma\tau}{2} - \mathcal{A}^\Delta \sinh \frac{\Delta\Gamma\tau}{2}, \\ I_-(\tau) &= \mathcal{C} \cos \Delta m_s \tau - \mathcal{S} \sin \Delta m_s \tau \\ \mathcal{N}_S &= \int [e^{-\Gamma\tau} (I_+(\tau) + \kappa(1 - 2\omega)I_-(\tau)) \otimes \mathcal{K}(\tau, t)] dt \\ \mathcal{N}_B &= \iint f_b(m_{\phi\gamma}, t) dm_{\phi\gamma} dt. \end{aligned}$$

The likelihood function is constructed as follows:

$$\mathcal{L}_0 = \left[\prod_{i=1}^{N_{ut}} P_0(m_i, t_i, \sigma_{t_i}), \right] \left[\prod_{i=1}^{N_{B_s}} P_{-1}(m_i, t_i, \sigma_{t_i}) \right] \left[\prod_{i=1}^{N_{\bar{B}_s}} P_1(m_i, t_i, \sigma_{t_i}) \right], \quad (\text{B.2})$$

where m_i, t_i, σ_{t_i} are the measured mass, proper time and proper time error for each event, correspondingly. For untagged analysis only one term in B.2 has to be considered.

The likelihood (B.2) function could be improved e.g. to take into account the overall integrated decay rates. Considering multiple tagging categories has the major potential to improve the results on \mathcal{S} and \mathcal{C} parameters which depend on the tagging. An improvement corresponding to 24% further statistics was seen by changing from a single to multiple tagging categories [15].

Appendix C: Calorimeter Calibration

The importance of Ecal calibration is illustrated by Figure 20. For Ecal miscalibrated at around $\sim 3\%$ one gets a $\sim 20\%$ increase of the signal width, which can be interpreted as the effective $\sim 20\%$ increase of the combinatorial background in the signal mass interval. In addition the relative contribution to the background from incompletely reconstructed B-decays rises. We also believe that the separation of single photons from the high energy “merged” π^0 -mesons degrades with degradation of Ecal calibration.

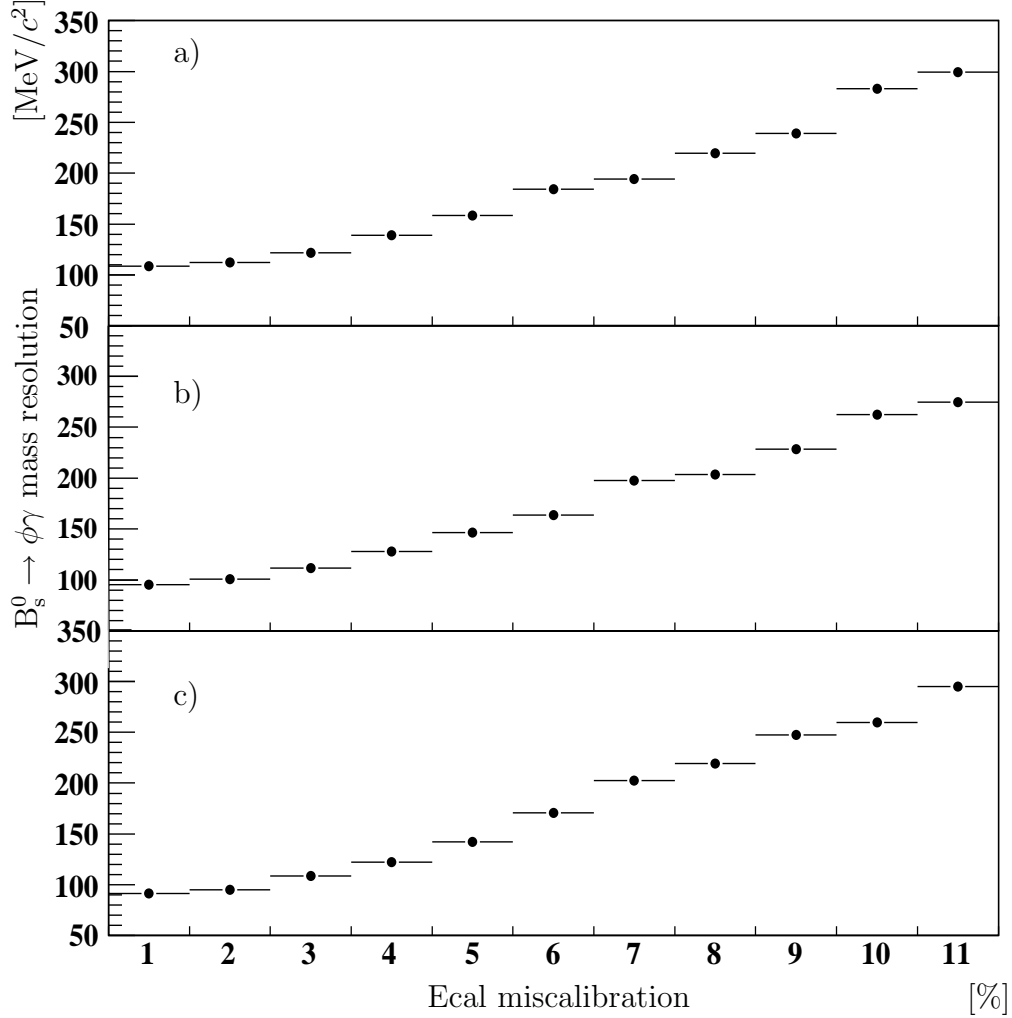


Figure 20: The mass resolution of $B_s^0 \rightarrow \phi\gamma$ peak as a function of Ecal miscalibrations for inner (a), middle (b) and outer (c) areas of the Calorimeter.

For the reconstruction of photon energy [64] both the energy deposited in electromagnetic calorimeter (Ecal) and the energy deposited in the Preshower detector (Prs) are used. Initial tests with cosmic particles of the individual modules before assembly of those modules in the Ecal shows that the initial light yield for different Ecal cells is

equalized within 4.3–8.0 % [65]. The phototube gains are remeasured in situ with LED’s. Monte Carlo studies show that the equalization of module response using the energy flow technique effectively allows to reduce the miscalibration of the modules at the level 3.7–5% for 20% initial miscalibration of Ecal. Moreover for the bulk of the modules the miscalibration does not exceed 4% [66].

A few different techniques have been discussed for the fine calibrations of the Ecal and Prs detectors:

- calibration of Ecal using minimum ionizing particles [67],
- iterative calibration of Ecal with neutral pions with no energy deposition in Prs detector,
- simultaneous calibration of Ecal and Prs with neutral pions using a “Millipede-like” multidimensional minimization procedure,
- simultaneous calibration of Ecal and Prs using electrons [67].

Also the calibration of the Prs detector using the the clear signal from a pair of minimal ionizing particles from photon conversion for the reconstructed photon candidates has been discussed.

Each technique has its own advantages and disadvantages and therefore a unique application range. The calibration with minimum ionizing particles and the iterative calibration with π^0 ’s allow to calibrate the Ecal only. The calibration of the Preshower detector requires other techniques. The “Millipede-like” calibrations with π^0 and e^\pm in theory both allow the simultaneous calibration of Ecal and Preshower detectors, but the procedures are more complicated and require the development of non-trivial code. Also from first principles one expects that the performance of these global methods to be very sensitive to the purity of the calibration sample and become rather fragile for samples with relatively low purity.

Also each calibration is efficient only for a certain energy range. For the selection of signal events a rather hard cut on the transverse energy of photons of the order of 2.8 GeV is usually applied [2, 5].

The calibration with minimum ionizing particles is rather simple but can be performed only for the middle and outer sections of the electromagnetic calorimeter [67]. The signals from minimum ionizing particles in the innermost part of the inner calorimeter are too small to be efficiently used for the calibration. The energy depositions from minimum ionizing particles are $\mathcal{O}(350 \text{ MeV})$ and the corresponding transverse energy is always less than 100 MeV, which is well outside of the most interesting energy region¹⁶. The calibration techniques based on $\pi^0 \rightarrow \gamma\gamma$ reconstruction are efficient for photons in the transverse energy range from $\sim 300 \text{ MeV}$ to $\sim 1.5 \text{ GeV}$. The overlapping of the electromagnetic showers from two photons effectively sets the transverse energy cutoff. The

¹⁶Note that ADC calibration is 2.5 MeV of transverse energy per ADC channel, and the noise is $\sim 3 \text{ MeV}$ per cell [9].

calibration techniques based on electrons are efficient in the energy range from ~ 1 GeV to 2–2.5 GeV. Here the transverse energy cutoff is set by the partial overlap of the electromagnetic shower from the initial electron and the shower from the bremsstrahlung photon emitted before the magnet.

Therefore we have no adequate calibration techniques which directly provides us with the calibration which fits into the most interesting transverse energy range. Here we need to rely on phototube linearity and the LED-based monitoring system [9, 68]. A complementary approach is discussed below.

As concerns the calorimeter calibration, one also needs to determine the numerous correction factors [64, 69] which are related to the spatial resolution of the Ecal. The leading corrections in the first approximation can be extracted from a detailed Monte Carlo study, however, the subleading, but small corrections are very sensitive to the actual distribution of the passive material in front of the Ecal and in between the Preshower and Ecal detectors. Currently we do not see a way to extract these corrections for the photons directly from the data, however similar corrections for electrons and positrons probably can be extracted from data. And by comparison with Monte Carlo one can try to calibrate the correction factors for the photons. Since these correction factors essentially reflect the actual shape of the electromagnetic shower for the given distribution of the passive material, they are considered to be constants and they need to be determined from data only once. Last but not at least the covariance matrix for the photon momentum needs to be evaluated properly. Current evaluation of this matrix result in some underestimation of the errors [2]. Such aspects are important for valid constraints and for the correct evaluation of the errors for the proper lifetime. These aspects are not discussed further here.

Iterative Ecal calibration with π^0

The iterative calibration of the electromagnetic calorimeter using the $\pi^0 \rightarrow \gamma\gamma$ peak in hadronic environment has been successfully used by the HERA-B Collaboration [70, 71] as the main calibration technique. It has been demonstrated that it gives a precise and robust Ecal calibration. This calibration does not rely on information from the other subdetectors, in particular it is tracking independent. It also has been shown that this calibration is fast and can be performed using very high rate of events available within the online environment.

The technique is based on the basic idea of the multiplicative energy correction coefficients and the direct relation between the energy shift of the photon and the shift of the visible position of π^0 peak:

$$m_{\gamma\gamma}^2 = 2E_1^\gamma E_2^\gamma (1 - \cos \theta_{\gamma\gamma}) \quad (\text{C.1})$$

If one assumes that the shift in the reconstructed mass of π^0 is due to one photon only, e.g. the first photon, one gets:

$$\frac{\delta m_{\gamma\gamma}}{m_{\gamma\gamma}} = \frac{1}{2} \frac{\delta E_1^\gamma}{E_1^\gamma}.$$

From this identity one can get the calibration (correction) coefficient to be applied for the selected photon to get the right mass of π^0 :

$$\lambda = \frac{E^{\text{true}}}{E_{\gamma}^{\text{rec}}} = 1 - 2 \frac{\delta m_{\gamma\gamma}}{m_{\gamma\gamma}}. \quad (\text{C.2})$$

The photon reconstruction procedure [64, 72] guarantees that the central cell of the cluster (“seed”) always has the largest energy. Due to coarse structure of the Ecal, electromagnetic clusters rarely spread outside the direct neighbours of the “seed” cell. Moreover very often the seed cell contains the bulk of the energy of whole cluster, and one has the following relations:

$$E_{seed} > E_i \quad \text{always} \quad (\text{C.3a})$$

$$E_{seed} \gg \max E_i \quad \text{very often} \quad (\text{C.3b})$$

$$E_{seed} > \sum E_i \quad \text{often} \quad (\text{C.3c})$$

$$E_{seed} \gg \sum E_i \quad \text{not rare,} \quad (\text{C.3d})$$

where E_{seed} represent the energy deposited in the seed cell of the cluster, E_i stands for the energy deposited in non-“seed” cell, and the sum runs over all cells excluding the “seed” cell.

With a little simplification, the reconstructed energy of photon can be written as the sum of two terms [64, 73]:

$$E_{\gamma}^{\text{rec}} = E_{Prs} f_1(x_b, y_b) + (E_{seed} + \sum_{i \neq seed} E'_i) f_2(x_b, y_b), \quad (\text{C.4})$$

where f_1 and f_2 are some functions, E_{Prs} - energy deposited in Preshower detector, x_b and y_b are x- and y-coordinates of the weighted barycenter of cluster, and E'_i is the energy in the cell, corrected for the possible overlap with the neighbouring cluster, $E'_i \leq E_i$. The function f_2 takes into account the transversal non-uniformity of the response, and in particular the small corrections for the transversal energy leakage and it is rather close to unity: $f_2 = 1 + \mathcal{O}(2 \%)$.

The property (C.3) and equation (C.4) imply that very often E_{γ}^{rec} is rather close to E_{seed} , and for the photons which do not deposit the energy in Preshower detector, $E_{Prs} = 0$, they are roughly proportional. As a result one can use value of calibration coefficient λ , obtained for the reconstructed photon as an estimate for the miscalibration of the “seed” cell. The actual procedure can works as follows.

For each Ecal cell, we select the reconstructed photons which has no (or very small) energy deposition in Preshower detector and which has this cell as “seed” cell. Clearly for the given event one has at most one such photon. Then we make the pairs from the selected photon and all other photons in the event and plot the invariant mass of the pair. It has been shown that if the initial miscalibration of Ecal does not exceed 15 % one should see the peak in the vicinity of the nominal mass of π^0 meson. The actual signal-to-background ratio, \mathcal{S}/\mathcal{B} , depends on the initial miscalibration, the simulated event types

and the selection criteria. The photon pairs are selected if they satisfy the following criteria:

- the transverse energy of the photon is required to be in excess of 300 MeV,
- the transverse energy of the photon pair is required to be in excess of 800 MeV,
- the energy deposited in the Preshower cells in front of the cluster is less than 10 MeV.

We have used minimum bias events, accepted by the L0 trigger [74] and photons have been selected using “no hits in the SPD detector” as neutrality criteria instead of matching of Ecal clusters with the reconstructed tracks. Therefore this kind of calibration is essentially *track independent*.

One can fit this distribution with a Gaussian function to describe the π^0 -signal, and a polynomial to describe the background. Using the formula (C.2) one can extract the calibration coefficient from the deviation of the Gaussian mean from the nominal mass of the π^0 -meson. The obtained calibration coefficient is ascribed to all photons from this class. After the repetition of the procedure for all Ecal cells one has the estimates for the calibration coefficients for all cells. The situation improves with more iterations and it stabilizes after 5-10 iterations.

It has been shown that if one defines the calibration coefficient according to equation (C.2) the convergence is worse and moreover it has a tendency to oscillate. The reasons for such overcalibration are rather clear - we have assumed that the whole energy of the photon is miscalibrated with the same coefficient as the energy of the seed cell. The alternative, improved formula:

$$\lambda' = \frac{E^{\text{true}}}{E_{\gamma}^{\text{rec}}} = 1 - \frac{\delta m_{\gamma\gamma}}{m_{\gamma\gamma}} \quad (\text{C.5})$$

shows much better behaviour, more rapid convergence and it is more stable with respect to variation of \mathcal{S}/\mathcal{B} . Effectively this modified definition corresponds to prescription that only half of the shift in the invariant mass of di-photon is due to miscalibration of the “seed” cell for the one photon and only half of the energy of the photon is contained in “seed” cell. This redefinition looks rather natural and in practice drastically improves the convergence of the iterative procedure.

After 5-10 “primary” iterations the procedure stabilizes and no further improvement occurs. Then one needs to perform the reconstruction of the photons taking into account the new calibration constants and to reiterate again. It forms a set of “secondary” iterations. Essentially the purpose of this “secondary” iteration is to take into account the change of photon barycenter parameters x_b and y_b , reevaluate the function f_s from equation (C.4) and the angle $\theta_{\gamma\gamma}$ from equation (C.1). The total convergence occurs after 2-3 “secondary” iterations. The final miscalibration level ϵ_{cal} after three “secondary iterations” with ten “primary iterations” each for the initial 10 % miscalibration can be parameterized as:

$$\epsilon_{cal} = \frac{4 \%}{\sqrt{N_{\pi^0}/100}}, \quad (\text{C.6})$$

where N_{π^0} is a number of reconstructed π^0 per cell. The miscalibration level ϵ_{cal} reaches $\sim 1\%$ at $N_{\pi^0} \approx 2 \cdot 10^3$ and goes down to 0.4% for $N_{\pi^0} = 10^4$.

With the described selection criteria the average number of reconstructed π^0 per minimum bias event is 0.023. The efficiency is so low mainly due to cut on Preshower energy. Combining this number with the equation (C.6), one gets the estimate for number of events $N_{\mathcal{L}}$ required to achieve a certain miscalibration level:

$$N_{\mathcal{L}} \sim \frac{5 \cdot 10^8}{(\epsilon_{cal} [\%])^2} \quad (\text{C.7a})$$

$$\epsilon_{cal} \sim \frac{2.2\%}{\sqrt{N_{\mathcal{L}}/10^8}}. \quad (\text{C.7b})$$

However, the equations (C.7) should be used with the some care, since they assume some uniformity of π^0 distributions over the calorimeter surface. Clearly this distribution is not uniform and the good calibration of certain Ecal regions could be achieved with significantly smaller number of events. Moreover for the off-line environment, the available event sample is enriched by events with high activity and larger multiplicity of energetic π^0 's, therefore one can expect larger π^0 yields. The equations (C.7) could be rewritten in a term of data taking duration $t_{\mathcal{L}}$, assuming output rate from the on-line farm to be 2 kHz and the data taking efficiency $\epsilon_{\mathcal{L}}$:

$$t_{\mathcal{L}} \sim \frac{3 \text{ day}}{\epsilon_{\mathcal{L}} (\epsilon_{cal} [\%])^2}$$

$$\epsilon_{cal} \sim \frac{1.7\%}{\sqrt{\epsilon_{\mathcal{L}} t_{\mathcal{L}} [\text{day}]}}.$$

Taking $\epsilon_{\mathcal{L}} \sim 50\%$ one gets that one week of data taking is enough to achieve a miscalibration of around 1%.

It is worth to stress here that for precalibration one can also use photons with non-zero energy deposition in the Preshower detector. For this case one can accumulate significantly larger statistics of π^0 -mesons, and for such conditions π^0 rides significantly lower background level. However for such sample of photons the multiplicative calibration does not hold anymore. As a result the procedure does not allow to reach the good calibration accuracy and suffers from the convergency to the right calibration constant. However, it allows rather fast and efficient precalibration of Ecal detector up to few percent level, thus providing a good starting point for the ultimate calibration.

It is possible that one could combine the best features of both approaches and perform the calibration with a sample of π^0 -mesons, where only one photon has negligible energy deposition in the Preshower detector. This approach is under investigation now.

At high photon energy the two Ecal clusters from the $\pi^0 \rightarrow \gamma\gamma$ decay start to overlap and therefore one can not consider anymore both reconstructed photons to be independent. This effect of ‘‘overlapped’’ or ‘‘merged’’ π^0 s efficiently sets the upper range for this type of calibration to be ~ 1.5 GeV of transverse energy [64, 9]. The lower range is set by the transverse energy cut to suppress the combinatorial background from soft photons and noisy clusters and is 300 MeV of transverse energy.

Calorimeter calibration with electrons

A complementary approach to a combined Ecal and Preshower calibration is the calibration with electrons. The method relies heavily on the proper reconstruction of tracks and probably on the proper dE/dx -corrections for the track fit. The second vital prerequisite is the possibility to select a sample of clean electrons. It can be done either through usage of RICH detectors or through kinematic selection of electrons and positrons from $\gamma \rightarrow e^+e^-$ conversion. The method relies on the simultaneous “Millipede-like”-minimization of a global χ^2 with respect to unknown calibration coefficients for Ecal and Preshower cells. The main advantage of this method consists in straightforward non-iterative calibration procedure which can be performed “on the fly” during normal data-taking or with a dedicated calibration run.

Requiring isolated tracks at the Ecal entrance and performing electron candidates selection we get data set which can be used for direct calorimeter calibration (based on the $E_{\text{CALO}}/P_{\text{track}}$ ratio).

Requiring electron ID with RICH, $R = 30$ cm isolation from the nearest charged track, visible Prs energy ($E_{\text{Prs}} > 20$ MeV) and limited Hcal energy ($E_{\text{Hcal}} < 1.5$ GeV) for tracks with $p_{\text{track}} > 4$ GeV/ c , we get a sample purity of ~ 91 %, see Figure 21.

With mean number of electrons per cell of ~ 1000 , we can get a relative calibration precision of about ~ 0.4 % for all three Ecal regions. The electron candidates are distributed quite non-uniformly over the Ecal so we will need ~ 150 M events (passed L0 trigger) to have at least 1000 electrons per cell even in regions with lowest occupancy.

The number of required events can be significantly reduced if we will accept possible calibration precision at the level of ~ 1 %. In this case the mean number of events per cell is around 100.

The selection of electrons without the RICH detector is possible by exploiting dE/dx in the VELO detector. This requirement significantly reduces statistics and, finally, we will get data set with worse purity, see Figure 22.

The relative statistics reduction (with respect to the first scenario) is a factor of 25. So, we will need around 400M events to get calibration precision at the level of around 1%.

More work is required to study the convergence of the method, its sensitivity to selection criteria, the sample purity and the shape of the background. The possibility to calibrate the Preshower detector needs to be verified.

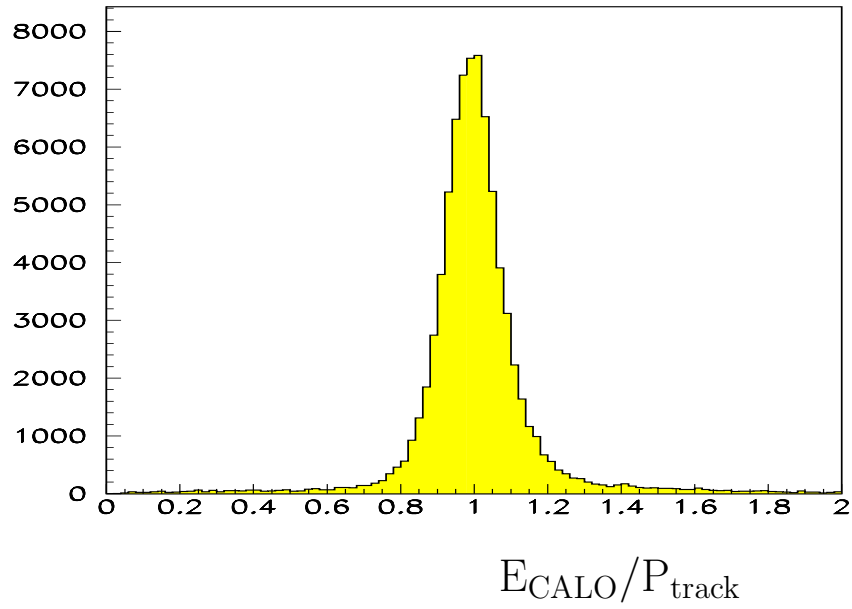


Figure 21: $E_{\text{CALO}}/P_{\text{track}}$ ratio for the electrons, selected using RICH information.

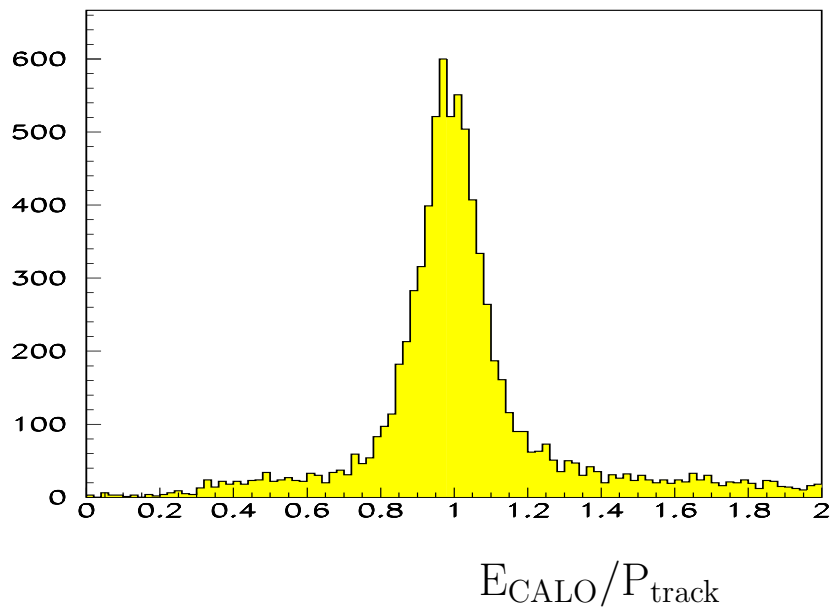


Figure 22: $E_{\text{CALO}}/P_{\text{track}}$ ratio for the electrons, selected using VELO information.

Calorimeter calibration for high- E_T photons

As has been mentioned in Section 4.3, each calibration method considered above has its own transverse energy range:

- the calibration with minimum ionizing particles allows to calibrate certain regions in Ecal for $15 \text{ MeV} \leq E_T^\gamma \leq 100 \text{ MeV}$,
- the iterative Ecal calibration with π^0 allows to calibrate Ecal in the transverse energy interval $300 \text{ MeV} \leq E_T^\gamma \leq 1.5 \text{ GeV}$,
- the calibration with e^\pm allows to calibrate Ecal up to the transverse energy 2 – 2.5 GeV,

which are outside the most interesting region $E_T^\gamma \geq 2.5 \text{ GeV}$. To propagate the calibration constants obtained for lower energy one needs to rely on phototube linearity¹⁷ and the LED-based monitoring system [9, 68]. But one needs to have an independent physical cross-check for the high energy calibration. The most appropriate candidate for such calibration channel is $\eta \rightarrow \gamma\gamma$. Due to the larger mass of η -meson compared to the π^0 the effective transverse energy cutoff occurs at significantly larger transverse energy, thus providing us access to isolated high energy photons. It has been shown that the peak $\eta \rightarrow \gamma\gamma$ is well visible, especially after vetoing $\pi^0 \rightarrow \gamma\gamma$ decays. The statistics of $\eta \rightarrow \gamma\gamma$ decays is more than order of magnitude less than the statistics of $\pi^0 \rightarrow \gamma\gamma$ events. In addition the $\eta \rightarrow \gamma\gamma$ peak sits on a larger combinatorial background due to larger available phase space for the diphoton system. These effects do not allow to use $\eta \rightarrow \gamma\gamma$ as a separate and efficient calibration channel. However, the position and the width of $\eta \rightarrow \gamma\gamma$ peak can be used for validation of Ecal calibration at a high transverse energy scale.

¹⁷The bulk of Ecal cells are equipped with phototubes with a nonlinearity term within $\pm 1 \%$ and the nonlinearity term does not exceed $\pm 2 \%$ for all phototubes [9].

Appendix D: Separation of photons and π^0 at high- E_T

The analysis of the remaining background events shows a large contribution from “merged” π^0 [2, 1]. The development of an algorithm that allows to suppress this contribution would result in a lower level of background and therefore more precise determination of the physical parameters. Also it could provide some additional robustness of the results with respect to unexpected imperfections.

It has been shown that it is possible to separate “merged” π^0 from single photons using the detailed shower shape analysis with the following variables:

$\langle r^2 \rangle = \text{Tr } \mathcal{S}$ - the average energy weighted squared distance for the individual cells in the cluster, this variable is equal to the trace of the 2×2 -matrix \mathcal{S} of the second momenta of the cluster [64]. This variable characterizes the overall size of the cluster.

$1 - \frac{\langle r^2 \rangle^2}{\langle r^4 \rangle}$, where $\langle r^4 \rangle$ is the average energy weighted r^4 for the individual cells in the cluster. This variable characterizes the importance of the tails of the cluster and is analogous to a kind of 2D-kurtosis.

$\kappa = \sqrt{1 - 4 \frac{\det \mathcal{S}}{\text{Tr}^2 \mathcal{S}}}$, where $\det \mathcal{S}$ is the determinant and $\text{Tr } \mathcal{S}$ is the trace of the matrix \mathcal{S} . This variable characterizes the ratio of eigenvalues for the matrix \mathcal{S} and therefore how stretched the cluster is.

$\alpha = \frac{\mathcal{S}_{xy}}{\sqrt{\mathcal{S}_{xx}\mathcal{S}_{yy}}}$ - this variable characterizes the orientation of the efficient ellipse, constructed from the second moments of the cluster, as well as how stretched the clusters are.

A likelihood function has been constructed from these variables properly taking into account their energy dependence, separately for all areas in Ecal.

For the testing sample of photons from $B^0 \rightarrow K^{*0}\gamma$ and merged π^0 from $B^0 \rightarrow K^{*0}\pi^0$ events, the achieved γ/π^0 separation is summarized in Table 10.

This technique could be further improved, e.g. for single photons the variable α should be slightly correlated with the azimuthal angle φ_γ of the photon: $\alpha \propto \sin 2\varphi_\gamma$, while for

Table 10: The efficiency of photon identification ϵ_γ and the probability of the “merged” π^0 misidentification as single energetic photon, ϵ_{π^0} for the different regions of the electromagnetic calorimeter.

Ecal region	ϵ_γ	ϵ_{π^0}
Inner	60 %	1.4 %
Middle	82 %	2.3 %
Outer	66 %	1.1 %

π^0 no such correlation is expected. Also the “Bulos” variable or the effective cluster mass, determined from the specialized “merged” π^0 reconstruction algorithm [64] can be used for π^0/γ separation.

A slightly simplified version of this technique, based on a linear Fisher discriminant [75] instead of the original likelihood ratio approach, is currently used for the High Level Trigger, see Section 3.2 and Reference [8].

References

- [1] P. Pakhlova and I. Belyaev, “Radiative B decays at LHCb”, CERN-LHCb-2003-090.
- [2] L. Shchutska, A. Golutvin and I. Belyaev, “Study of radiative penguin decays $B \rightarrow K^{*0}\gamma$ and $B_s \rightarrow \phi\gamma$ at LHCb”, CERN-LHCb-2007-030.
- [3] L. Shchutska *et al.*, “Probing the photon polarization in $B_s \rightarrow \phi\gamma$ at LHCb”, CERN-LHCb-2007-147.
- [4] L. Shchutska, “Probing the photon polarization in $B_s \rightarrow \phi\gamma$ at LHCb”, Master Theses, MIPT&ITEP/Moscow, Russia, 2008, CERN-THESIS-2008-095.
- [5] F. Legger, “Reconstruction of the decays $\Lambda_b \rightarrow \Lambda^0\gamma$ and $\Lambda_b \rightarrow \Lambda(1670)\gamma$ at LHCb”, CERN-LHCb-2006-012.
- [6] F. Legger, “Polarized radiative Λ_b decays at LHCb”, CERN-LHCb-2006-013.
- [7] F. Legger, “Contribution to the Development of the LHCb acquisition electronics and Study of polarized radiative Λ_b decays”, Ph.D. Theses, EPFL/Lausanna, Switzerland, 2006, CERN-THESIS-2006-044.
- [8] K. Senderowska, M. Witek and A. Żurański, “HLT Electromagnetic Alley”, CERN-LHCb-PUB-2000-001.
- [9] S. Amato *et al.*, “LHCb calorimeters: Technical Design Report”, CERN-LHCC-2000-036.
- [10] J. Albrecht *et al.*, “Measurement of mixing-induced \mathcal{CP} -violation in $B_s^0 \rightarrow \phi J/\psi$ ”, Chapter 4 of this document.
- [11] T. Blake *et al.*, “Analysis of the decay $B_d^0 \rightarrow K^{*0}\mu^+\mu^-$ ”, Chapter 6 of this document.
- [12] D. Martinez Santos *et al.*, “Analysis of the decay $B_s^0 \rightarrow \mu^+\mu^-$ ”, Chapter 5 of this document.
- [13] M. Adinolfi *et al.*, “The tree-level determination of γ ”, Chapter 2 of this document.
- [14] A. Bates *et al.*, “Charmless charged two-body B decays”, Chapter 3 of this document.
- [15] M. Calvi, O. Leroy and M. Musy, “Flavour tagging algorithms and performances in LHCb”, CERN-LHCb-2007-058.
- [16] M. Neubert, “Radiative B decays: Standard candles of flavor physics”, arXiv:hep-ph/0212360.
- [17] G. Buchalla, A. J. Buras and M. E. Lautenbacher, “Weak Decays Beyond Leading Logarithms”, *Rev. Mod. Phys.* **68**, 1125 (1996).

- [18] T. Feldmann, “Recent developments in soft-collinear effective theory,” arXiv:hep-ph/0610192.
- [19] A. Ali, B. D. Pecjak and C. Greub, “ $B \rightarrow V\gamma$ Decays at NNLO in SCET,” Eur. Phys. J. C **55** (2008) 577.
- [20] B.D. Pecjak, “Theory Review of Exclusive Rare Radiative Decays,” arXiv:0806.4846 [hep-ph].
- [21] A.J. Buras, “Minimal flavor violation,” Acta Phys. Polon. B **34** (2003) 5615.
- [22] Lattice 2008, The XXVI International Symposium on Lattice Field Theory, Williamsburg, Virginia, USA, 14-19 July 2008, <http://conferences.jlab.org/lattice2008/>
- [23] A.L. Kagan and M. Neubert, “Isospin breaking in $B \rightarrow K^*\gamma$ decays,” Phys. Lett. B **539** (2002) 227.
- [24] B. Grinstein, Y. Grossman, Z. Ligeti and D. Pirjol, “The photon polarization in $B \rightarrow X\gamma$ in the standard model”, Phys. Rev. D **71**, 011504 (2005).
- [25] B. Grinstein and D. Pirjol, “The \mathcal{CP} asymmetry in $B^0(t) \rightarrow K_S^0\pi^0\gamma$ in the standard model”, Phys. Rev. D **73**, 014013 (2006).
- [26] M. Matsumori and A.I. Sanda, “The Mixing-induced CP asymmetry in $B \rightarrow K^*\gamma$ decays with perturbative QCD approach”, Phys. Rev. D **73**, 114022 (2006).
- [27] P. Ball and R. Zwicky, “Time-dependent CP Asymmetry in $B \rightarrow K^*\gamma$ as a (Quasi) Null Test of the Standard Model”, Phys. Lett. B **642**, 478 (2006).
- [28] D. Atwood, M. Gronau and A. Soni, “Mixing-induced CP Asymmetries in Radiative B Decays in and beyond the Standard Model”, Phys. Rev. Lett. **79**, 185 (1997).
- [29] L. Everett, G.L. Kane, S. Rigolin, L.-T. Wang and T.T. Wang, “Alternative approach to $b \rightarrow s\gamma$ in the uMSSM”, JHEP **0201**, 022 (2002).
- [30] J.-P. Lee, “Photon polarization with anomalous right-handed top couplings in $B \rightarrow K_{res}\gamma$ ”, Phys. Rev. D **69**, 014017 (2004).
- [31] K. Agashe, G. Perez and A. Soni, “B-factory Signals for a Warped Extra Dimension”, Phys. Rev. Lett. **93**, 201804 (2004).
- [32] T. Gershon and A. Soni, “Null tests of the Standard Model at an International Super B Factory”, [arXiv:hep-ph/0607230].
- [33] M. Gronau, Y. Grossman, D. Pirjol and A. Ryd, “Measuring the Photon Helicity in Radiative B Decays”, Phys. Rev. Lett. **88**, 051802 (2002).

- [34] M. Gronau and D. Pirjol, “Photon polarization in radiative B decays”, Phys. Rev. D **66**, 054008 (2002).
- [35] V.D. Orlovsky and V.I. Shevchenko, “On the photon polarization in radiative $B \rightarrow \phi K \gamma$ decay”, Phys. Rev. D **77**, 093003 (2008).
- [36] T. Mannel and S. Recksiegel, “Flavour Changing Neutral Current Decays of Heavy Baryons: The Case $\Lambda_b \rightarrow \Lambda \gamma$ ”, J. Phys. G **24**, 979 (1998).
- [37] G. Hiller and A. Kagan, “Probing for New Physics in Polarized Λ_b decays at the Z”, Phys. Rev. D **65**, 074038 (2002).
- [38] F. Legger and T. Schietinger, “Photon helicity in $\Lambda_b \rightarrow p K \gamma$ decays” Phys. Lett. B **645**, 204 (2007).
- [39] D. Melikhov, N. Nikitin and S. Simula, “Probing right-handed currents in $B \rightarrow K^* \ell^+ \ell^-$ transitions”, Phys. Lett. B **442**, 381 (1998).
- [40] C.S. Kim, Y.G. Kim, C.D. Lü and T. Morozumi, “Azimuthal angle distribution in $B \rightarrow K^* (\rightarrow K \pi) \ell^+ \ell^-$ at low invariant $m(\ell^+ \ell^-)$ region”, Phys. Rev D **62**, 034013 (2000).
- [41] Y. Grossman and D. Pirjol, “Extracting and using photon polarization information in radiative B decays”, JHEP **0006**, 029 (2000).
- [42] F. Krüger, L.M. Sehgal, N. Sinha and R. Sinha, “Angular distribution and CP asymmetries in the decays $\bar{B} \rightarrow K^- \pi^+ e^- e^+$ and $\bar{B} \rightarrow \pi^- \pi^+ e^- e^+$ ”, Phys. Rev. D **61**, 114028 (2000).
- [43] J. Lefrancois and M.-H. Schune, “Measuring the photon polarization in $b \rightarrow s \gamma$ using $B \rightarrow K^* e^+ e^-$ decay channel”, CERN-LHCb-PUB-2009-008.
- [44] D. Atwood, T. Gershon, M. Hazumi and A. Soni, “Mixing-induced CP violation in $B \rightarrow P_1 P_2 \gamma$ in search of clean new physics signals”, Phys. Rev. D **71** (2005) 076003.
- [45] F. Muheim, Y. Xie and R. Zwicky, “Exploiting the width difference in $B_s \rightarrow \phi \gamma$ ”, Phys. Lett. B **664**, 174 (2008).
- [46] R. Ammar *et al.*, “Evidence for penguins: First observation of $B \rightarrow K^*(892) \gamma$ ”, Phys. Rev. Lett. **71** (1993) 674.
- [47] T. Hurth and T. Mannel, “Direct CP violation in radiative B decays”, AIP Conf. Proc. **602**, 212 (2001).
- [48] B. Aubert *et al.*, “Measurement of branching fractions, and CP and isospin asymmetries, for $B \rightarrow K^* \gamma$ ”, Phys. Rev. D **70**, 112006 (2004).

- [49] M. Nakao *et al.*, “Measurement of the $B \rightarrow K^*\gamma$ branching fractions and asymmetries”, Phys. Rev. D **69**, 112001 (2004).
- [50] T. E. Coan *et al.*, “Study of exclusive radiative B meson decays”, Phys. Rev. Lett. **84**, 5283 (2000).
- [51] C. Amsler *et al.*, “Review of Particle Physics,” Phys. Lett. B **667**, 1 (2008) and 2009 partial update for the 2010 edition.
- [52] E. Barberio *et al.*, “Averages of b-hadron and c-hadron Properties at the End of 2007”, arXiv:0808.1297 [hep-ex].
- [53] A. Drutskoy *et al.*, “Observation of radiative $B \rightarrow \phi K\gamma$ decays”, Phys. Rev. Lett. **92**, 051801 (2004).
- [54] J. Wicht *et al.*, “Observation of $B_s \rightarrow \phi\gamma$ and Search for $B_s \rightarrow \gamma\gamma$ Decays at Belle,” Phys. Rev. Lett. **100**, 121801 (2008).
- [55] B. Aubert *et al.*, “Measurement of B decays to $\phi K\gamma$ ”, Phys. Rev. D **75**, 051102 (2007).
- [56] B. Aubert *et al.* “Measurement of Time-Dependent CP Asymmetry in $B^0 \rightarrow K_S^0\pi^0\gamma$ Decays,” Phys. Rev. D **78**, 071102 (2008).
- [57] Y. Ushiroda *et al.*, “Time-dependent CP asymmetries in $B^0 \rightarrow K_S^0\pi^0\gamma$ transitions”, Phys. Rev. D **74**, 111104 (2006).
- [58] B. Aubert *et al.*, “Branching Fractions and CP-violating asymmetries in Radiative B Decays to $\eta K\gamma$,” Phys. Rev. D **79**, 011102 (2009).
- [59] J. Li *et al.*, “Time-dependent CP Asymmetries in $B^0 \rightarrow K_S^0\rho^0\gamma$ Decays,” Phys. Rev. Lett. **101**, 251601 (2008).
- [60] Y. Ushiroda *et al.*, “Time-Dependent **CP**-Violating Asymmetry in $B^0 \rightarrow \rho^0\gamma$ Decays,” Phys. Rev. Lett. **100** (2008) 021602.
- [61] S. Behari, “Measurement of B hadron lifetimes at CDF”, arXiv:0810.3758 [hep-ex].
- [62] V. Gligorov, J. Rademaker, “Monte Carlo Independent Lifetime Fitting at LHCb in Lifetime Biased Channels”, CERN-LHCb-2007-053.
- [63] M. Calvi *et al.*, “Lifetime unbiased selection of $B_s^0 \rightarrow J/\psi\phi$ and related control channels $B^0 \rightarrow J/\psi K^{*0}$ and $B^+ \rightarrow J/\psi K^+$ ”, LHCb-2009-025.
- [64] O. Deschamps *et al.*, “Photon and neutral pion reconstruction”, CERN-LHCb-2003-091.

- [65] A. Aref'ev *et al.*, “Design, construction, quality control and performance study with cosmic rays of modules for the LHCb electromagnetic calorimeter”, CERN-LHCb-2007-148.
- [66] K. Voronchev and I. Belyaev, “Energy flow calibration of LHCb ECAL”, CERN-LHCb-2006-051.
- [67] I. Korolko *et al.*, “On the possibility of *in situ* calibration of LHCb calorimeters”, CERN-LHCb-2000-051.
- [68] Y. Gilitsky, I. Korolko and E.A. Melnikov, “The monitoring system for the LHCb ECAL”, CERN-LHCb-2003-151.
- [69] H. Terrier and I. Belyaev, “Particle identification with LHCb calorimeters”, CERN-LHCb-2003-092.
- [70] G. Avoni *et al.*, “The electromagnetic calorimeter of the HERA-B experiment”, Nucl. Instrum. Meth. A **580** (2007) 1209.
- [71] O. Igonkina *et al.*, “On-line π^0 calibration of ECAL”, HERA-B/00-103.
- [72] V. Breton, N. Brun and P. Perret, “A clustering algorithm for the LHCb electromagnetic calorimeter using a cellular automaton”, CERN-LHCb-2001-123.
- [73] C. Gonzáles Bañó, “Study of the LHCb Calorimeter Calibration using Photons and Electrons”, Ph.D. Theses, Universidad de Barcelona, 2008, CERN-THESES-2008-058.
- [74] R. Antunes-Nobrega *et al.*, “LHCb trigger system: Technical Design Report”, CERN-LHCC-2003-031.
- [75] R.A. Fisher, “The Use of Multiple Measurements in Taxonomic Problems”, Annals of Eugenics, **7** (1936) 179.